Plant Physiology Preview. Published on February 19, 2015, as DOI:10.1104/pp.114.253377

FYVE1 is essential for vacuole biogenesis and intracellular trafficking in *Arabidopsis thaliana*

Cornelia Kolb[1], Marie-Kristin Nagel[1], Kamila Kalinowska[1], Jörg Hagmann[2], Mie Ichikawa[3], Franziska Anzenberger[1], Angela Alkofer[1], Masa H. Sato[3], Pascal Braun[1], and Erika Isono[1,4]

[1] Plant Systems Biology, Technische Universität München, Emil-Ramann-Str.4, 85354 Freising, Germany

[2] Max Planck Institute for Developmental Biology, Department of Molecular Biology, Spemannstr. 35, 72076 Tübingen, Germany

[3] Department of Life and Environmental Sciences, Kyoto Prefectural University Shimogamonakaragi-cho 1-5, Sakyo-ku, Kyoto, 606-8522 Japan

[4] **Corresponding author:**
Erika Isono
E-mail: erika.isono@wzw.tum.de
phone: ++49 (0)8161 712875
fax: ++49 (0)8161 712886.

Running Title:
FYVE1 is essential for vacuole formation

One Sentence Summary:
A phospholipid-binding protein regulates intracellular trafficking and vacuole formation.

Abstract

The plant vacuole is a central organelle that is involved in various biological processes throughout the plant life cycle. Elucidating the mechanism of vacuole biogenesis and maintenance is thus the basis for our understanding of these processes. Proper formation of the vacuole has been shown to depend on the intracellular membrane trafficking pathway. Although several mutants with altered vacuole morphology have been characterized in the past, the molecular basis for plant vacuole biogenesis has yet to be fully elucidated. With the aim to identify key factors that are essential for vacuole biogenesis, we performed a forward genetics screen in *Arabidopsis thaliana* and isolated mutants with altered vacuole morphology. The *vacuolar fusion defective 1 (vfd1)* mutant shows seedling lethality and defects in central vacuole formation. *VFD1* encodes FYVE1, a Fab1, YOTB, Vac1 and EEA1 (FYVE)-domain containing protein that has been implicated in intracellular trafficking. FYVE1 localizes on late endosomes and interacts with SH3-domain-containing proteins. Mutants of *FYVE1* are defective in ubiquitin-mediated protein degradation, vacuolar transport and autophagy. Altogether, our results show that FYVE1 is essential for plant growth and development and place FYVE1 as a key regulator of intracellular trafficking and vacuole biogenesis.

Introduction

The plant vacuole is the largest organelle in a plant cell, in which proteins, metabolites and ions can be stored or sequestered. The vacuole is essential for plant development and growth and is directly or indirectly involved in various biotic and abiotic stress responses [reviewed in (Zhang et al., 2014)]. The vacuole is also the central organelle for degradation of endocytic and autophagic protein substrates through the activity of vacuolar proteases. In both degradation pathways, substrates are transported to the vacuole by intracellular membrane trafficking. In endocytic degradation, plasma membrane-localized proteins are targeted to the vacuole for degradation by endosomes [reviewed in (Reyes et al., 2011)]. This process is important, among others, to control the abundance of plasma membrane receptors and thus downstream signaling events. Autophagic degradation is mainly involved in nutrient recycling. During this process, cytosolic proteins and organelles are either selectively or non-selectively transported by double membrane autophagosomes to the vacuole to be degraded [reviewed in (Liu and Bassham, 2012)]. Vacuolar transport defines an intracellular transport pathway by which *de novo* synthesized proteins or metabolic compounds are carried to the vacuole by vesicle transport [reviewed in (Drakakaki and Dandekar, 2013)].

In yeast, forward genetic screens aimed at finding mutants with defective vacuolar transport or vacuolar morphology have identified more than 30 *VACUOLAR PROTEIN SORTING (VPS) and VACUOLAR MORPHOLOGY (VAM)* genes (Banta et al., 1988; Raymond et al., 1992; Wada and Anraku, 1992). Closer analyses have shown that many of these mutants have defects both in protein sorting and in vacuole biogenesis, suggesting a close link between these processes. *vps* and *vam* mutants were classified into six mutant classes according to their phenotypes. The strategic success of these screens has been confirmed when later studies revealed that many of the genes categorized in the same mutant class were coding for subunits of the same protein complexes. Among them were complexes important for membrane transport and fusion events, such as the endosomal sorting complex required for transport (ESCRT)-I, -II and -III [reviewed in (Henne et al., 2011)] or the homotypic fusion and vacuole protein sorting (HOPS) complex [reviewed in (Balderhaar and Ungermann, 2013)].

Sequence homologs of most yeast *VPS* genes can be found in the Arabidopsis genome (Sanderfoot and Raikhel, 2003; Bassham et al., 2008), and

some of them were reported to be involved in intracellular trafficking as well as vacuole biogenesis. For example, the Arabidopsis *vacuoleless* (*vcl*)/*vps16* mutant is embryo lethal and lacks lytic vacuoles (Rojo et al., 2001). VPS16 is a subunit of the HOPS complex, suggesting that membrane fusion events mediated by VCL/VPS16 are also important for plant vacuole biogenesis. Several other Arabidopsis *vps* mutants were also shown to have altered vacuole morphology at the mature embryo stage (Shimada et al., 2006; Sanmartín et al., 2007; Ebine et al., 2008; Yamazaki et al., 2008; Zouhar et al., 2009; Shahriari et al., 2010; Ebine et al., 2014), showing that there is a conserved mechanism regulating vacuolar transport and vacuole biogenesis. However, in contrast to yeast, in which mutants without vacuole or severe biogenesis defects are viable, plant vacuoles seem to be essential for plant development.

We have previously shown that defects in the deubiquitinating enzyme (DUB) ASSOCIATED MOLECULE WITH THE SH3 DOMAIN OF STAM 3 (AMSH3) also lead to a severe vacuole biogenesis defect (Isono et al., 2010). *AMSH* homologs do not exist in budding yeast but are conserved in animals and plants. Our previous studies have shown that AMSH3 can directly interact with ESCRT-III subunits (Katsiarimpa et al., 2013). ESCRT-III is a multiprotein complex that is essential for multivesicular body (MVB) sorting (Winter and Hauser, 2006) and hence for plant growth and development (Haas et al., 2007; Spitzer et al., 2009; Katsiarimpa et al., 2011; Cai et al., 2014). AMSH proteins regulate intracellular trafficking events including endocytic degradation, vacuolar transport and autophagic degradation through its interaction with ESCRT-III (Isono et al., 2010; Katsiarimpa et al., 2011; Katsiarimpa et al., 2013; Katsiarimpa et al., 2014). Prior to our characterization of the *amsh3* mutant, AMSH proteins had not been implicated in vacuole biogenesis. Thus, we reasoned that there might be additional, yet unidentified, factors important for regulating vacuole biogenesis in plants. Further we reasoned that other mutants with a defect in vacuole biogenesis, analogous to *amsh3*, might also exhibit seedling lethality

Thus, with the goal to identify and characterize these factors, we carried out a two-step mutant screen. We first selected seedling lethal mutants from an ethyl methansulfonate (EMS)-mutagenized population and then examined the vacuole morphology in these mutants. The isolated mutants were designated *vacuolar fusion defective (vfd). vfd1* is affected in the expression of a functional Fab1, YOTB, Vac1

and EEA1 (FYVE) domain-containing FYVE1 protein. FYVE1 was originally identified *in silico* as one of 16 FYVE domain-containing proteins in Arabidopsis with no apparent homologs in yeast and mammals (van Leeuwen et al., 2004). FYVE domains bind phosphatidylinositol 3-phosphate (PIP3), a phospholipid that is a major constituent of endosomal membranes. Hence, FYVE domain-containing proteins are implicated in intracellular trafficking [reviewed in (van Leeuwen et al., 2004) (Wywial and Singh, 2010)]. In a previous work, we have shown that a null mutant of FYVE1, *fyve1-1*, is defective in IRON-REGULATED TRANSPORTER1 (IRT1) polarization and that *FYVE1* is essential for plant growth and development (Barberon et al., 2014). A very recent publication describing the same mutant has shown that FYVE1/FREE1 is also important for the early and late endosomal trafficking events (Gao et al., 2014). In this study, we show that FYVE1 is also regulating ubiquitin-dependent membrane-protein degradation, vacuolar transport, autophagy and vacuole biogenesis. Altogether, our results point toward FYVE1 being a key component of the intracellular trafficking machinery in plants.

Results

vacuolar fusion defective (vfd) 1 shows seedling lethality and has defects in central vacuole formation

In order to identify additional essential factors that are involved in vacuolar biogenesis and intracellular trafficking processes in Arabidopsis, we conducted a forward genetic screen. For this purpose, we EMS-mutagenized seeds of a tonoplast marker GFP-*∂*-TONOPLAST INTRINSIC PROTEIN (*∂*TIP)-expressing Col-0 line (Cutler et al., 2000). M1 plants were then self-pollinated and seeds of approximately 3,500 M1 plants were collected in pools containing 5 plants each. Next, we carried out a two-step phenotype screen on M2 seedlings. We first searched for a seedling lethal phenotype similar to *amsh3*, a mutant of the ESCRT-III-associated DUB AMSH3, that we have previously characterized (Isono et al., 2010; Katsiarimpa et al., 2014). Subsequently, we examined the identified mutant candidates under the confocal microscope for altered vacuole morphology, typically for a smaller vacuole size in a confocal section. We named these mutants *vacuole fusion defective* (*vfd*) after the apparent defect in vacuolar fusion to form a large central vacuole in the mutants.

vfd1 is one of the thus identified mutants and shows recessive inheritance of the mutant phenotype. Homozygous *vfd1* mutants either did not germinate or showed seedling lethality after germination (Figure 1A). *vfd1* vacuoles appeared to be much smaller in comparison to the wild type (Figure 1B) when visualized with the tonoplast marker GFP-∂TIP, indicating that *vfd1* shares the characteristic phenotype of the previously described *amsh3* mutant.

VFD1 encodes the FYVE domain-containing FYVE1 protein

To identify the locus that was responsible for the *vfd1* phenotype, we performed Small Sequence Length Polymorphism (SSLP)-based mapping. Marker analysis has revealed that the *vfd1* mutation is located within a 6 Mbp region on the short arm of chromosome 1. We next performed whole-genome sequencing to analyze mutations within the identified region. Sequencing analysis revealed twelve non-synonymous typical EMS transitions in twelve genes within the rough-mapped region. To identify the gene causing the *vfd1* phenotype, we next carried out a complementation assay in *vfd1*. Only *35Spro:FYVE1* (At1g20110) could complement the seedling lethal mutant phenotype of *vfd1*, indicating that a nonsense mutation (C415T) in *FYVE1* is responsible for the *vfd1* phenotype (Figure 1C and Supplemental Figure 1). FYVE1 is a plant-specific FYVE-domain containing protein that is regulating the polarity of the iron transporter IRT1 and MVB-sorting (Barberon et al., 2014; Gao et al., 2014).

To confirm that dysfunction of *FYVE1* indeed causes the *vfd1* phenotype, we analyzed a transposon insertion line of *FYVE1* (Figure 2A). We designated this mutant allele *fyve1-1* (Barberon et al., 2014). The same line was later referred to as *free1* by Gao et al (Gao et al., 2014). *fyve1-1* showed a seedling lethal phenotype similar to *vfd1* (Figure 2B). qRT-PCR analysis has shown that *fyve1-1* has only residual transcript levels of the truncated *FYVE1* gene (Figure 2C). Besides its seedling lethality, *fyve1-1* also shows degenerated root surface structures as seen in Figure 2D, indicating that FYVE1 is essential for proper root development. To verify that *fyve1-1* and *vfd1* are allelic, we crossed a heterozygous *fyve1-1* with a heterozygous *vfd1* plant and analyzed the F1 progeny. The seedling phenotypes of transheterozygotes were identical to that of *fyve1-1* or *vfd1* (Supplemental Figure 2M), indicating the *fyve1-1* and *vfd1* are allelic to each other. Thus, we designated *vfd1* as *fyve1-2.*

To examine whether *fyve1-1* shows altered vacuole morphology like *fyve1-2*, we crossed GFP-∂TIP into a *fyve1-1* background and examined the vacuole phenotype in wild-type and *fyve1-1* homozygous mutant seedlings. Instead of a large central vacuole that can be visualized in a wild-type epidermis cell, *fyve1-1* mutants accumulate seemingly smaller vacuoles in the cytosol (Figure 2E), corroborating that FYVE1 is crucial for proper vacuole biogenesis. Furthermore, both the seedling and vacuole phenotype of *fyve1* mutants resemble the previously characterized *amsh3* mutant (Supplemental Figure 2A-L), suggesting that FYVE1 and AMSH3 might function in the same cellular pathway.

Vacuoles of *fyve1-1* show altered morphology

To further establish the vacuole phenotype of *fyve1-1*, we analyzed BCECF-AM-stained vacuoles of wild-type and *fyve1-1* seedlings by confocal microscopy. For the comparison, 2-day-old wild type seedlings were chosen due to the similar size with the fyve1-1 mutant (Supplemental Figure 2B, C and I). On a normal confocal image, vacuoles of *fyve1-1* seem to be fragmented in comparison to the wild type and it appears as if many small vacuoles are filling the cytosol of *fyve1-1* cells (Figure 3A and C). To analyze the vacuole morphology in more details, we performed a 3D-reconstruction analysis by surface rendering on Z-stack images of wild-type and *fyve1-1* vacuoles from cells of approximately the same size. Surface rendering suggests that the small vacuoles in *fyve1-1* are, in fact, interconnected with each other forming a complex tubular structure (Figure 3B and D). This result suggests that FYVE1 is important for the determination of vacuolar morphology.

Ubiquitinated membrane-associated proteins accumulate in *fyve1-1*

It was previously shown that mutations in ESCRT-III subunits and AMSH proteins or treatment with trafficking inhibitors lead to the accumulation of ubiquitinated proteins (Isono et al., 2010; Katsiarimpa et al., 2013; Cai et al., 2014; Katsiarimpa et al., 2014) and that most of the accumulated proteins are found in the microsomal fraction (Katsiarimpa et al., 2014). To establish whether a defect in the FYVE1 protein also affects degradation of ubiquitinated proteins, we conducted immunodetection assays with an ubiquitin antibody on total cell extracts of wild-type, *fyve1-1*, and *fyve1-2* seedlings. Both *fyve1* mutants accumulated ubiquitinated proteins at a higher level than in the wild type (Figure 4A and B), indicating that FYVE1 is necessary for the

degradation of ubiquitinated substrates. Accumulation of ubiquitinated proteins is restored to the wild-type level in a *35Spro:FYVE1* expressing plant (Figure 4A), indicating that *FYVE1* is indeed affecting the global ubiquitin profile. As previously reported (Gao et al., 2014), *fyve1-1* mutants accumulated ubiquitinated proteins at high levels (Figure 4B). To examine whether the accumulated ubiquitinated proteins are membrane-bound, we performed fractionation by ultracentrifugation to gain microsomal (P100) and soluble (S100) fractions. Immunoblotting showed that the majority of the ubiquitinated proteins were detected in the microsomal fraction (P100) (Figure 4C). Together, these results suggest that FYVE1 is involved in the removal of ubiquitinated proteins that are associated with endomembranes.

fyve1-1 is defective in vacuolar transport

Beside the endosomal trafficking of ubiquitinated proteins, vacuolar protein sorting is another pathway that transports vesicle cargos to the vacuole. To investigate whether *fyve1-1* is defective in protein transport to the vacuole, we examined the behavior of the model vacuolar cargo GFP-CT24 (Nishizawa et al., 2003). GFP-CT24 contains the signal peptide for vacuolar targeting in seeds, and was previously shown to cause green seed fluorescence in mutants defective in vacuolar transport (Fuji et al., 2007). We therefore analyzed GFP-CT24 containing seeds from wild type and heterozygous *fyve1-1* plants, and observed seeds with strong green fluorescence in the *fyve1-1* heterozygous line (Figure 5A). Seeds with strong fluorescence corresponded to *fyve1-1* homozygous mutants as verified by PCR-based genotyping (Supplemental Figure 4). For the following experiments, we used this phenotype to distinguish between *fyve1-1* homozygous and non-homozygous seeds. In wild-type or heterozygous embryos, signals of GFP-CT24 completely overlapped with the autofluorescence of the seed storage vacuoles, whereas in *fyve1-1* homozygous embryos, GFP-CT24 signals were observed exclusively in the intercellular spaces (Figure 5B). Autofluorescence of the seed storage vacuoles was still observed in the homozygous *fyve1-1* mutants and the altered morphology of seed storage vacuoles was apparent (Figure 5B). This result shows that FYVE1 is involved in vacuole biogenesis already at the mature embryo stage.

To further investigate the vacuolar transport of seed storage proteins, we next analyzed the protein abundance of endogenous seed storage proteins, and chose two major seed storage proteins, 2S albumin and 12S globulin. In total extracts

derived from seeds, precursor proteins of both 2S albumin and 12S globulin accumulated in *fyve1-1* (Figure 5C-E). These precursor proteins are readily processed in the wild type upon delivery to the vacuole, thus suggesting that *fyve1-1* is affected in proper sorting of these storage proteins to the vacuole. The abundance of GFP-CT24 was also examined at the protein level. When compared to the wild type, *fyve1-1* also accumulated higher amounts of GFP-CT24 (Figure 5C and F), which is probably due to the increased stability of GFP-CT24 in the intercellular spaces (Fuji et al., 2007). As the accumulation of precursor proteins is a strong indication of defective vacuolar processing, these data indicate that FYVE1 is involved in proper vacuolar transport of seed storage proteins.

fyve1-1 has defects in the autophagy pathway

Recent reports have shown that intracellular membrane trafficking is closely related to autophagy (Katsiarimpa et al., 2013; Kulich et al., 2013), a pathway that eliminates and recycles cellular components. In autophagic degradation, the cytosol or selected cargo proteins marked with ubiquitin are sequestered by double membranes to form autophagosomes. Autophagosomal membranes contain AUTOPHAGY 8 (ATG8), an ubiquitin-like protein that is activated by a cascade of enzymes similar to the ubiquitin pathway (Yoshimoto et al., 2004). After engulfing of contents and closure of the double membrane, autophagosomes are targeted to the vacuole where upon fusion with the vacuolar membrane, the content is released and degraded by vacuolar proteases. ATG8 is a constitutive structural component of the autophagosome, and therefore an ideal marker to monitor autophagy. In a*msh3* mutants, ATG8 has been shown to accumulate (Isono et al., 2010). Since *fyve1* mutants are phenotypically similar to *amsh3* mutants, we wondered whether *fyve1* mutants are also altered in the autophagy pathway.

To test this possibility, we analyzed the steady-state level of ATG8 and NEIGHBOR of BRCA1 GENE 1 (NBR1). Whereas ATG8 is present in most types of autophagosomes, NBR1 is specific to selective autophagy and acts as a cargo adapter protein (Svenning et al., 2011). Both autophagy markers accumulated in autophagy-defective mutant seedlings of *atg7-2* (Hofius et al., 2009) and *atg10-1* (Phillips et al., 2008). *atg7-2* and *atg10-1* are mutants of the E1-activating and E2-conjugating enzymes of the autophagic pathway, respectively. Similar to the *atg* mutants, ATG8 and NBR1 also accumulated in *fyve1-1* (Figure 6), indicating that

fyve1-1 is also defective in the autophagy pathway. Since not only ATG8 but also NBR1 accumulated in *fyve1-1,* FYVE1 is involved in both selective- and non-selective autophagy pathway.

FYVE1 is localized to the cytosol and to late endosomes

FYVE1 was previously shown to bind to phosphoinositides and localize to late endosomal vesicles together with the 2xFYVE marker and two late endosome (LE)/MVB markers Rha1 and VACUOLE SORTING RECEPTOR2 (VSR2) (Barberon et al., 2014; Gao et al., 2014). We analyzed the subcellular localization of a functional *UBQ10pro:GFP-FYVE1* construct (Barberon et al., 2014) with further markers. As previously reported, GFP-FYVE1 signals appeared in the cytosol as well as in small vesicles in the cytosol. Among the total of 257 GFP-FYVE1 vesicles, 31.6% colocalized with the LE/MVB marker mCherry-ARABIDOPSIS RABGTPase 7 (ARA7) (Geldner et al., 2009) whereas only 7.4 % of the GFP-FYVE1 vesicles showed overlap with the early endosome (EE)/trans-Golgi network (TGN) marker SYNTAXIN OF PLANTS43 (SYP43)-mRFP (Ebine et al., 2008) (Figure 7A and D). To further analyze this localization, we treated the seedlings with the ARF-GEF inhibitor brefeldin A (BFA) and the PI3K and PI4K-inhibitor Wortmannin (WM). After 45 minutes of 50 µM BFA-treatment, mRFP-SYP43 accumulated in BFA-bodies (Figure 7B and C) while the localization of GFP-FYVE1 remained unaffected. In contrast, after 45 minutes of 33 µM WM-treatment, both mCherry-ARA7 and GFP-FYVE1 were localized to the WM-induced ring like structure (Figure 7D and E), corroborating the observation, that FYVE1 is associated to LE/MVBs.

To investigate the membrane association of the FYVE1 biochemically, we generated an anti-FYVE1-specific antibody. The antibody recognized overexpressed GFP-FYVE1, but failed to detect the endogenous FYVE1 protein in plant total extracts (data not shown). Therefore we used the GFP-FYVE1 line for fractionation and immunodetection analysis. Total extracts (S13) of wild-type and GFP-FYVE1 seedlings were subjected to ultracentrifugation to obtain membrane-(P100) and soluble (S100) fractions. GFP-FYVE1 was detected in both soluble- and membrane fractions (Figure 7D), suggesting that GFP-FYVE1 is not exclusively associated with membranes. This result is in accordance with the observation that GFP-FYVE1 is localized in both vesicles and the cytosol and also suggests the possibility that GFP-FYVE1 recycles between the cytosol and the membrane.

FYVE1 interacts with SH3P2 and SH3P3

Arabidopsis has 16 FYVE domain-containing proteins whose molecular and biological functions are diverse (van Leeuwen et al., 2004; Wywial and Singh, 2010; Hirano et al., 2011; Serrazina et al., 2014). The FYVE-domain serves to bind membranes, but it is the interaction with other proteins that is important in defining the role of a given FYVE domain protein. Therefore, to better understand the molecular framework surrounding FYVE1 function, we wanted to identify interacting proteins of FYVE1. To this end, we performed a Yeast Two-Hybrid (YTH) screen against 12,000 Arabidopsis proteins encoded by sequence verified ORFs (Consortium, 2011; Weßling et al., 2014) using FYVE1 as a bait. We used a truncated variant of FYVE1 lacking the FYVE domain [FYVE1(ΔFYVE)] because we wanted to rule out the possibility that FYVE1 might also be targeted to membranes in yeast, and thereby interfere with the efficiency of the YTH screen. The YTH screen, in which the bait was screened in a binary test against all individual ORFs in the collection, was carried out independently three times. To ensure reliability and reproducibility of the interactions, only interactor candidates that appeared at least in two of the three independent experiments were further considered. Since *fyve1* mutants showed severe phenotypes in intracellular trafficking, we decided to first focus on proteins with a known function in this pathway. One of these was SH3P3, which has been described as a protein implied in intracellular trafficking in Arabidopsis (Lam et al., 2001).

SH3P1, SH3P2 and SH3P3 are the three SH3-domain containing proteins that were previously reported to be involved in clathrin-mediated endocytosis (Lam et al., 2001). Among the three, SH3P2 and SH3P3 share the highest sequence homology. To establish whether SH3P1 and SH3P2 can also interact with FYVE1, we performed a targeted YTH analysis. To increase the confidence in the interaction, we sub-cloned the FYVE1(ΔFYVE) into another YTH vector and analyzed the interaction between FYVE1(ΔFYVE) and SH3P1, SH3P2 and SH3P3. SH3P2 and SH3P3, but not SH3P1, showed interaction with FYVE1, indicating that they share a common interaction partner in FYVE1 (Figure 8 and Supplemental Figure 3). Moreover, as the ΔFYVE variant was able to interact with these proteins, the FYVE domain is not involved in the interaction between these proteins.

FYVE1 co-localizes with SH3P2 on class E compartments

We next examined whether these proteins function on the same cellular compartments. SH3P1 was previously shown to localize on clathrin-coated vesicles by immunoelectron microscopy (Lam et al., 2001). To examine the localization of SH3P2, we generated a *SH3P2pro:SH3P2-GFP* plant line. We noticed that SH3P2-GFP localizes on vesicles, on the plasma membrane and in the cytosol. To analyze the nature of these vesicles, we crossed the SH3P2-GFP-expressing line with CLC-mKO, mRFP-SYP43 and mCherry-ARA7-expressing plants. SH3P2-GFP signals showed strong overlap with CLC-mKO (69.0 %, n=619) (Figure 9A). We detected also partial co-localization of SH3P2-GFP with the EE/TGN-marker mRFP-SYP43 (16.0 %, n=162) and with the LE/MVB-marker mCherry-ARA7 (7.2 %, n=158) (Figure 9B and C), albeit with much lower frequency. These results show that the majority of SH3P2 molecules functions on CLC-positive vesicles, though a fraction of SH3P2 molecules localize to the cytosol and to other vesicles.

Since GFP-FYVE1 showed co-localization with ARA7 (Figure 7) and since we detected interactions between FYVE1 and SH3P2, we further investigated the possibility that SH3P2 can transiently associate with LE/MVBs together with FYVE1. To this end, we further examined the localization of SH3P2-GFP upon WM-treatment and upon inhibition of ESCRT-III function. WM is an inhibitor of PI3- and PI4-kinases and thereby inhibits endosomal trafficking. 120 min of WM treatment caused accumulation of the LE/MVB marker mRFP-ARA7 to WM-induced compartments. However, under this condition, the localization of SH3P2-GFP remained unaffected (Figure 9D to F). This result confirms that SH3P2, unlike ARA7, is not a stable component of LE/MVBs.

To test whether the localization of SH3P2 is affected by the inhibition of ESCRT-III function, we next examined the behavior of SH3P2-GFP together with the ESCRT-III associated mCherry-AMSH3 upon co-expression of an inactive SUPPRESSOR OF K+ TRANSPORT GROWTH DEFECT1 (SKD1). SKD1 is a AAA-ATPase that is essential for the disassembly of the ESCRT-III complex. Upon expression of the ATPase-inactive SKD1(EQ) variant, ESCRT-III disassembly is inhibited and enlargement of the MVB occurs (Haas et al., 2007), leading to the formation of so called class E compartments.

Because the expression of SKD1(EQ) is toxic *in planta*, we investigated the effect of SKD1(EQ) in Arabidopsis cell culture-derived protoplasts. This system was

successfully used to stabilize and visualize transient interaction between ESCRT-III and its interacting AMSH3 protein, both of which show uniform cytosolic localization that was not affected by WM treatment (Katsiarimpa et al., 2011). To verify the specificity of the effect caused by SKD1(EQ), we analyzed the co-expression of SKD1(WT) and SKD1(EQ) with CLC-mKO, mRFP-SYP41 and mRFP-ARA7. As a control, ESCRT-III subunits VPS2.1 and VPS24.1 were co-transformed. SKD1(EQ)-induction specifically affected the localization of the LE/MVB marker ARA7 causing ARA7 to accumulate in class E compartments together with ESCRT-III subunits (Supplemental Figure 5). In contrast, CLC and the EE/TGN marker SYP43 did show accumulation on class-E compartments (Supplemental Figure 5). This experiment shows that at least in this experimental system, SKD1(EQ)-induction specifically accumulates ARA7- and ESCRT-III related proteins to class E compartments.

When SH3P2-GFP and mCherry-AMSH3 were co-expressed with SKD1(EQ), but not with SKD1(WT), we observed that SH3P2-GFP accumulated together with mCherry-AMSH3 on class E compartments (Figure 9G to I). Since AMSH3 was shown to interact directly with ESCRT-III, (Katsiarimpa et al., 2011), and since ESCRT-III was shown to localize on LE/MVBs (Scheuring et al., 2011), this result suggests that there must be at least a transient interaction of SH3P2-GFP with LE/MVB. SH3P2-GFP also co-localized with TagRFP-FYVE1 (Figure 9J and K) on SKD1(EQ)-induced class E compartments, suggesting that they can function together on an (late)endosomal compartment sensitive to SKD1(EQ).

Altogether, our results indicate that FYVE1 is essential for ubiquitin-mediated protein degradation, vacuolar transport, autophagy and proper vacuole biogenesis and/or maintenance. FYVE1 localizes on late endosomes and, like the ESCRT-III-interacting DUB AMSH3, is recruited together with its interactor SH3P2 to ESCRT-III-positive class E compartments. Through the interaction with other proteins that are involved in intracellular trafficking, as illustrated by the interaction with SH3P2, FYVE1 could play a central role in the regulation of these key cellular processes and hence is pivotal for plant growth and development (Figure 10).

Discussion

FYVE1 as an essential factor in vacuole biogenesis and endomembrane trafficking

With the goal to identify new proteins involved in vacuole biogenesis, we used a forward genetics approach and screened an EMS-mutagenized population for

mutants with altered vacuole morphology. In our study, we report the identification and characterization of the *vfd1(fyve1-2)* and *fyve1-1* mutants and show that FYVE1 is an essential component in vacuole biogenesis. FYVE1 was recently reported as an interactor and regulator of the polarity of the iron transporter IRT1 and it was also shown that overexpression of FYVE1 leads to hypersensitivity towards low-iron conditions (Barberon et al., 2014). In another recent publication, it was shown that the *fyve1-1* mutant (named *free1* by the authors) is defective in MVB sorting and ubiquitin-dependent protein degradation in Arabidopsis (Gao et al., 2014). Our characterization of the *fyve1* mutants revealed that, in addition to the vacuole biogenesis defect, they are also affected in the degradation of ubiquitinated proteins associated to membranes, vacuolar transport and autophagy, indicating that FYVE1 has a pleiotropic role in endomembrane trafficking.

Vacuoles in Arabidopsis root cells have been shown to change their morphology dynamically during cell elongation (Viotti et al., 2013). *fyve1-1* cells do not contain a large central vacuole but instead have a complex tubular structure of vacuoles that is reminiscent of wild-type vacuoles in the meristematic cells (Viotti et al., 2013). The process of central vacuole formation is not well understood yet, but it most certainly requires homotypic membrane fusion events. The HOPS tethering complex, soluble *N*-ethylmaleimide-sensitive factor (NSF) attachment receptors (SNAREs) and RAB7 GTPases are described as proteins involved in this process in yeast [reviewed in (Wickner, 2010)]. The fact that mutants of the Arabidopsis homologs of these factors also display altered vacuole morphology (Rojo et al., 2001; Sanmartín et al., 2007; Ebine et al., 2008; Zouhar et al., 2009; Ebine et al., 2014) suggests that the same proteins are involved in vacuolar membrane fusion events in plants. Since it is essential for these proteins to be properly targeted to the correct endomembrane, FYVE1 dysfunction and the defect in intracellular trafficking as a consequence might impact the transport of these tethering/fusion factors to the vacuolar membrane. This in turn might cause defects in vacuolar membrane fusion, causing altered vacuolar morphology in *fyve1* mutants.

Role of FYVE1 in vacuolar protein transport

Different cargos of the vacuolar sorting pathway employ distinct transport routes to the vacuole in a RAB5- and RAB7-activity dependent process (Cui et al., 2014; Ebine et al., 2014; Singh et al., 2014). Storage protein sorting also relies on the proper

function of vacuolar sorting receptors (Fuji et al., 2007) and the fact that the *fyve1-1* mutant mis-sorted seed storage proteins indicates that FYVE1 function might affect the localization, transport or activity of these proteins. Alternatively, the vacuole biogenesis defect in *fyve1-1* might alter the vacuolar membrane lipid or protein composition in the first place. Therefore, in *fyve1-1*, regulators of vacuolar protein transport might not be able to recognize the tonoplast, their target membrane, causing defects in vacuolar protein transport.

FYVE1 harbors a FYVE domain, a well-characterized domain that can bind to phospholipids, especially PI3P (van Leeuwen et al., 2004). In contrast to yeast and mammals, in which PI3P is found also in early endosomes, PI3P was reported to be enriched in late endosomes in plants (Vermeer et al., 2006). This is in accordance with the localization of FYVE1 on late endosomes as well as its reported function in MVB-sorting (Gao et al., 2014). The presence of GFP-FYVE1 in the cytosol suggests that the FYVE-domain alone is not enough for a constitutive binding of FYVE1 to vesicles. Depending on the protein structure outside of the FYVE domain and the presence of catalytic domains, FYVE domain-containing proteins can play variable roles in endomembrane-related pathways. FYVE1 does not contain obvious domains with catalytic activity, implying that it probably executes its cellular function by interacting with other proteins of the pathway, for example by serving as a scaffold to recruit other proteins onto the endosomal membrane. Both *fyve1* mutants used in this work cannot produce transcripts with a functional FYVE domain. Thus even if the truncated proteins are stably expressed, they would not be able to bind to endomembranes, which may render the protein non-functional.

FYVE1 function in different intracellular trafficking processes

Although it is evident from recently published studies (Barberon et al., 2014; Gao et al., 2014) and the data presented in this study that FYVE1 is key to many membrane trafficking processes, the molecular function of FYVE1 still remains to be elucidated. Since FYVE1 does not have an apparent functional domain except for the FYVE domain and a C-terminal coiled-coil domain, it is informative to identify interacting proteins of FYVE1 to better understand its molecular function. We therefore carried out a YTH screen using FYVE1 as a bait, and identified two SH3-domain containing proteins SH3P2 and SH3P3 as interactors of FYVE1.

The Arabidopsis genome contains three genes that code for SH3-doamin containing proteins, SH3P1, SH3P2 and SH3P3. SH3P1 was originally reported to localize on clathrin-coated vesicles and interact with the clathrin disassembling factor Auxillin (Lam et al., 2001). Our results show that although almost 70 % of vesicle-localized SH3P2 are on CLC-positive vesicles, a small portion of SH3P2 can localize to the LE/MVB. Though the interaction of FYVE1 and SH3P2 may be of a transient nature, they may regulate membrane transport together at the LE/MVB. In addition to the function at LE/MVB, as assumed from its localization, FYVE1 might also play a role in different types of endosomes. A recent publication has shown that FYVE1 can interact with the ESCRT-I component VPS23.1 *in vitro* and *in vivo* (Gao et al., 2014). The ability of FYVE1 to interact with VPS23.1 and with ubiquitin led to the assumption that FYVE1 acts as an ESCRT-I interacting ubiquitin adapter protein. Although we could detect only a little overlap between GFP-FYVE1 and the EE/TGN marker, we noticed that GFP-FYVE1 is also localized in the cytosol. This might suggest that the cytosolic fraction of FYVE1 can transiently interact with early endosomal components and regulates endocytosis in association with these. The fact that the *fyve1* mutant is defective in a plethora of intracellular trafficking pathways supports this hypothesis.

fyve1-1 showed accumulation of ATG8 that is a structural component of autophagosomes, indicating that the mutant has defects in the autophagic pathway. In addition, it also showed stabilization of NBR1, indicating that not only bulk autophagy but also selective autophagy is inhibited in this mutant. It has been shown that Arabidopsis mutants in the ESCRT-III and ESCRT-III-related *amsh* mutants (Isono et al., 2010; Katsiarimpa et al., 2013) as well as an Exocyst mutant (Kulich et al., 2013) have defects in autophagy. These reports indicate that there is a strong correlation between the functionality of basic intracellular trafficking and autophagic degradation. Since FYVE1 seems to play a central role in different aspects of endomembrane trafficking as described in this report, we can assume that these defects in turn could affect the autophagy pathway. Interestingly, SH3P2 was reported to interact with ATG8 proteins, to localize on autophagosomes and to regulate autophagy (Zhuang et al., 2013). Thus, in regard to the interaction of FYVE1 with SH3P2, FYVE1 could also be involved directly in the regulation of autophagic degradation.

fyve1 mutants phenocopy the *amsh3* mutant in regard to their general seedling morphology, vacuolar structure, defects in ubiquitinated cargo degradation, vacuolar protein sorting and autophagy. Both proteins are predicted to function at the late endosomes, although, in contrast to AMSH3 (Katsiarimpa et al., 2011), it was shown that FYVE1 does not interact with ESCRT-III subunits (Gao et al., 2014). It might still be possible that AMSH3 and FYVE1 act together in the regulation of ubiquitin-mediated proteolysis in the endosomal pathway. It is our future subject to investigate the relationship between FYVE1 and AMSH3 and to elucidate the molecular framework surrounding FYVE1 function in intracellular trafficking in order to decipher its role in plant growth and development.

Materials and methods

Plant material and media: All plant experiments were performed with *Arabidopsis thaliana*. Wild type Columbia-0 (Col-0) and Nossen (No-0) were used as controls for experiments with *vfd1/fyve1-2* and *fyve1-1*, respectively. transposon insertion line of *FYVE1* in No-0, designated *fyve1-1* (RIKEN pst18264), was described previously (Barberon et al., 2014). *fyve1-1* was genotyped with primers EI511, EI512 and Ds5-2a. Sequences of primers used for genotyping are listed in Supplemental Table 1. Genotyping-PCR products were analyzed using the QIAxcel Advanced System (QIAGEN). Plant transformations were performed using the floral dip method (Clough and Bent, 1998). Seedlings were grown in continuous light at 110 µmol m^{-2} s^{-1} light intensity. Standard Murashige and Skoog (MS) growth medium (Duchefa Biochemie) supplemented with 1% sucrose (2.15 g/L MS and 2.3 mM MES, pH 5.7) was used to grow seedlings and adult plants were grown in soil. Arabidopsis root cell culture was used to produce protoplasts for transient transformation and localization analysis as described previously (Katsiarimpa et al., 2011).

Identification of the *VFD1/FYVE1* gene: To map the *VFD1/FYVE1* locus, an F2-mapping population was generated by crossing a *vfd1* heterozygous plant (Col-0) with a wild-type L*er* plant. F1 plants were allowed to self-pollinate, and F2 progenies were screened for the *vfd1* phenotype. Genomic DNA was isolated and subjected to SSLP-based marker analysis. SSLP analysis restricted the *vfd1* map interval to a 6 Mbp region defined by markers F16J7-TRB and NGA392. To identify the region

carrying the causative mutation, genomic DNA was pooled from approximately 100 F2 mutant seedlings that had been obtained from a single back-cross of *vfd1* to Col-0. A paired-end sequencing library was prepared using the NEBNext DNA Sample Prep Reagent Set for Illumina (New England Biolabs) according to the manufacturer's instructions. The library was subjected to 100 bp-paired-end whole-genome sequencing using a single lane on an Illumina Hiseq2000 machine. The resulting reads were mapped against the Col-0 reference genome (TAIR9) using GenomeMapper (Schneeberger et al., 2009) and single nucleotide polymorphisms (SNPs) were called using SHORE (Ossowski Genome Res 2008). SNPs were filtered by read support (minimum 10), concordance (>80%), uniqueness and typical EMS transitions (C>T, G>A), resulting in 216 potential EMS-induced mutations on the whole genome. Using plotting functions of SHOREmap (Schneeberger et al., 2009), we found that almost half of them clustered on the left arm of chromosome 1 indicating low recombination in this region. Annotating the SNPs resulted in twelve non-synonymous mutations within the previously rough-mapped region.

Cloning procedures: All primers used for cloning and sub-cloning are listed in Supplemental Table 1. *35Spro:FYVE1* was generated by cloning the ORF of *FYVE1* with primers CK40 and CK41 into pGWB414 (Nakagawa et al., 2007) using Gateway technology (Invitrogen). *UBQ10pro:GFP-FYVE1* and *35Spro:TagRFP-FYVE1* were generated by cloning the PCR-amplified *FYVE1* ORF into pUBN-GFP-DEST (Grefen et al., 2010) and pGWB461 (Nakagawa et al., 2007), respectively. *35Spro:GFP-SH3P2* was obtained by PCR-amplifying the ORF of *SH3P2* with the primer pair MN53 and MN54 and inserting the resulting PCR-product into 35S-GW-GSP (MPI Cologne). *SH3P2pro:SH3P2-GFP* was generated by amplifying a genomic fragment of SH3P2 with primers SH3P2-up5 fw and SH3P2-dw3 rv and cloning the resulting PCR-product into pGWB404 (Nakagawa et al., 2007). *GAD-FYVE1 (∆FYVE)* for the YTH ORF screen was created by cloning the coding region of *FYVE1* without the FYVE domain using primers CK41, CK131, CK140 and CK141 into pDEST-DB (Mukhtar et al., 2011). For the verification of the YTH results, FYVE1 (∆FYVE) was amplified with the primer pair VC11 and VC12 and cloned into pGADT7 (Clontech). ORFs of *SH3P1*, *SH3P2* and *SH3P3* were amplified with primer pairs MN215 and MS8, MS11 and MS12 or MS9 and MS10, respectively, and cloned into pGBKT7 (Clontech). The ORF of *CLC2* was amplified using primers EI223 and EI224 and

cloned into *pUBQ10pro:RFP-CLC*. *AMSH3pro:mCherry-AMSH3* was created by replacing the *YFP* of *AMSH3pro:YFP-AMSH3* (Katsiarimpa et al., 2011) with *mCherry*. For antigen production, a *FYVE1* fragment was amplified with the primer pair EI528 and EI529 and cloned into pET21a (Novagen). *35Spro:SKD1(WT)*, *35Spro:SKD1(EQ), UBQ10pro:YFP-VPS2.1, UBQ10pro:YFP-VPS24.1* (Katsiarimpa et al., 2011), *35Spro:mRFP-SYP41* and *35Spro:mRFP-ARA7* (Ueda et al., 2004; Uemura et al., 2004) were described previously.

qRT-PCR and RT-PCR: Sequences of primers used for qRT-PCR (EI541 and EI542) and RT-PCR (CK104 and CK105) are listed in Supplemental Table 1. Total RNA was extracted from 7-day-old seedlings with a NucleoSpin RNA plant kit (Machery-Nagel). 1 µg of total RNA was reverse transcribed with an oligo(dT) primer and M-MulV reverse transcriptase (Fermentas) following the manufacturer's instructions. Quantitative real-time PCR was performed using iQ SYBR Green Supermix (Bio-Rad) in a CFX96 real-time system cycler (Bio-Rad). A 45-cycle two-step amplification protocol (10 s at 95°C, 25 s at 60°C) was used for all measurements.

EMS mutagenesis: Mutagenesis of GFP-∂TIP-expressing Col-0 seeds with EMS was performed as described previously (Weigel and Glazebrook, 2001). Progeny of about 3,500 M1 plants were screened for seedling lethality and for the *vfd* phenotype.

Protein Extraction, Immunoblotting, and Antibodies: Yeast total proteins were extracted according to a previously described protocol (Kushnirov, 2000). SDS-PAGE and immunoblotting were performed according to standard methods. Plant total protein extracts were prepared in extraction buffer (50 mM Tris- HCl, pH 7.5, 150 mM NaCl, 0.5% Triton X-100, and protease inhibitor cocktail [Roche]). For seed storage protein analysis NuPAGE 4-12% Bis-Tris gels (Life Sciences) were used. For fractionation, total extracts were centrifuged for 20 min at 13,000 g at 4˚C, and the supernatant (S13) was further centrifuged for 1 h at 100,000 g at 4˚C in a Sorvall MTX 500 benchtop ultracentrifuge (Thermo Scientific) to obtain the soluble (S100) and microsomal (P100) fractions. Antibodies used in this study were as follows: anti-ATG8 (Thompson et al., 2005), anti-GFP (Invitrogen), anti-CDC2 (Santa Cruz), anti-GAL4BD (Santa Cruz), anti-HA (Roche), anti-NBR1 (Svenning et al., 2011), anti-UB (P4D1) (Santa Cruz), anti-UGPase (Agrisera), anti-H^+-ATPase (Agrisera), anti-2S

and anti-12S (Shimada et al., 2003). An anti-FYVE1 antibody was raised in rabbits (Eurogentec) using a truncated FYVE1 protein (aa 36-280) that was purified from bacteria as an antigen.

Microscopy: To visualize the vacuole, seedlings were incubated with 5 µM BCECF-AM (Molecular Probes) for 1 hour. WM (Applichem) treatment was performed at a concentration of 33 µM for 120 minutes at room temperature. To visualize vacuoles, seedlings were incubated with 5 µM BCECF-AM (Molecular Probes, Invitrogen) and 0.02% Pluronic F-127 (Molecular Probes, Invitrogen) for 1 hour at room temperature in darkness. GFP- or TagRFP/mCherry/mRFP/mKO-fused proteins and BCECF staining were analyzed with an FV-1000/IX81 confocal laser scanning microscope (Olympus) equipped with GaAsP detectors (Olympus) and a UPlanSApo X60/1.20 (Olympus) objective using the 488-, 559- and 405-nm laser line, respectively. For surface rendering of wild-type and *fyve1-1* vacuoles, 90 Z-stacks images with 0.2 µm step size were obtained. Images were subsequently processed using Imaris 7 (Bitplane). Surface rendering was performed with the following parameters. The surface area detail level was set to 0.122 µm and signal intensity threshold was set to 80. Seeds expressing GFP-CT24 were photographed using the Olympus BZX16 stereomicroscope (Olympus). For scanning electron microscopy, Seedling roots were observed directly with a TM-3000 scanning electron microscope (Hitachi).

Yeast two-hybrid screen and interaction analysis: A YTH screen using GAD-FYVE1(ΔFYVE) (cloned into pDest-AD-CYH2) as bait was performed as described previously (Dreze et al) against a collection of 12,000 GBD-fused Arabidopsis ORFs (Weßling et al., 2014) using Y8800/Y8930 (*MATa/α*, *leu2-3,112 trp1-901 his3-200 ura3-52 gal4D gal80D GAL2-ADE2 LYS2::GAL1-HIS3 MET2::GAL7-lacZ cyh2^R*) strains. The bait was screened by yeast mating against a collection of 12,000 Arabidopsis ORFs fused to the Gal4 DNA binding domain (GBD) (Weßling et al., 2014). The screen was done as a binary 1:1 screen, *i.e.* the single AD bait was screened against 12,000 individual DB clones in our collection and growth was assayed using the *HIS3* and *ADE2* reporters, the former using 1mM 3-Amino-1,2,4-triazole (3-AT) to suppress background growth. This screen was carried out independently for three times and candidates were sequence verified. Only partners that appeared in at least two of the experiments were selected for further analysis.

For a targeted analysis of protein pairs, GBD-fused SH3P1, SH3P2, SH3P3 (cloned into pGBKT7) and GAD-fused FYVE1(ΔFYVE) (cloned into pGADT7) were transformed into Y8800 cells and double transformants were grown on selective plates to test auxotrophic growth.

Accession Numbers: Sequence data from this article can be found in the Arabidopsis Genome Initiative Database under the following accession numbers: *ACT8* (AT1G49240), *AMSH3* (AT4G16144), *ATG8a* (AT4G21980), *ATG8b* (AT4G04620), *ATG8c* (AT1G62040), *ATG8d* (AT2G05630), *ATG8e* (AT2G45170), *ATG8f* (AT4G16520), *ATG8g* (AT3G60640), *ATG8h* (AT3G06420), *ATG8i* (AT3G15580), *FYVE1* (At1g20110), *NBR1* (AT4G24690), *SH3P1* (At1g31440), *SH3P2* (AT4g34660) and *SH3P3* (At4g18060).

Supplemental Material:

Supplemental Figure 1: Complementation of *vfd1(fyve1-2).*

Supplemental Figure 2: Phenotypes of *fyve1* in comparison with *amsh3*.

Supplemental Figure 3: Protein expression analysis of Y2H clones.

Supplemental Figure 4: Genotyping of GFP-CT24 expressing seeds

Supplemental Figure 5: Effect of SKD1(EQ) expression on endosomal markers.

Supplemental Table 1: Primers used in this study.

Acknowledgements

We would like to thank Detlef Weigel and Markus Schmid (MPI Tübingen) for the whole genome sequencing of *vfd1(fyve1-2)*. We also like to thank Christa Lanz and Jens Riexinger (MPI Tübingen) for technical assistance in Illumina sequencing and Jerome Moriniere, Vanessa Chmielewski and Markus Schneider (TU München) for assistance in the project. We are grateful to Richard Vierstra (University of Wisconsin-Madison), Tomoo Shimada and Ikuko Hara-Nishimura (Kyoto-University), Tomohiro Uemura, Takashi Ueda and Akihiko Nakano (University of Tokyo), Niko Geldner (Université Lausanne), Tsuyoshi Nakagawa (Shimane University), Christopher Grefen (Tübingen University) and Mike Blatt (University of Glasgow) for kindly sharing published materials and RIKEN-BRC for the *fyve1-1* mutant seeds. We are also grateful to Emi Ito (University of Tokyo), Carina Behringer, Balaji Enugutti,

Farhah Assaad and Alexander Steiner (Technische Universität München), for technical advice and Frédéric Brunner (Tübingen University) for critical reading of the manuscript. This work was supported by grants from the Deutsche Forschungsgemeinschaft SFB924 (A06) to E.I. and SFB924 (A10) to P.B. and by a-grant-in-aid for Scientific Research on Innovative Areas (No. 25119720) from the Ministry of Education, Culture, Sports, Science and Technology Japan to M.H.S..

Author contributions

C.K., M.-K.N., K.K., F.A., A.A., M.I. and E.I. performed experiments and analyzed the data, J.H. perforemd NGS data analysis, M.-H.S., P.B., and E.I. designed experiments, and E.I. designed the project and wrote the manuscript.

References

Balderhaar HJ, Ungermann C (2013) CORVET and HOPS tethering complexes - coordinators of endosome and lysosome fusion. J Cell Sci **126:** 1307-1316

Banta LM, Robinson JS, Klionsky DJ, Emr SD (1988) Organelle assembly in yeast: characterization of yeast mutants defective in vacuolar biogenesis and protein sorting. J Cell Biol **107:** 1369-1383

Barberon M, Dubeaux G, Kolb C, Isono E, Zelazny E, Vert G (2014) Polarization of IRON-REGULATED TRANSPORTER 1 (IRT1) to the plant-soil interface plays crucial role in metal homeostasis. Proc Natl Acad Sci U S A **111:** 8293-8298

Bassham DC, Brandizzi F, Otegui MS, Sanderfoot AA (2008) The Secretory System of Arabidopsis. American Society of Plant Biologists

Cai Y, Zhuang X, Gao C, Wang X, Jiang L (2014) The Arabidopsis Endosomal Sorting Complex Required for Transport III Regulates Internal Vesicle Formation of the Prevacuolar Compartment and Is Required for Plant Development. Plant Physiol **165:** 1328-1343

Clough SJ, Bent AF (1998) Floral dip: a simplified method for Agrobacterium-mediated transformation of *Arabidopsis thaliana*. Plant J **16:** 735-743

Consortium AIM (2011) Evidence for network evolution in an Arabidopsis interactome map. Science **333:** 601-607

Cui Y, Zhao Q, Gao C, Ding Y, Zeng Y, Ueda T, Nakano A, Jiang L (2014) Activation of the Rab7 GTPase by the MON1-CCZ1 Complex Is Essential for PVC-to-Vacuole Trafficking and Plant Growth in Arabidopsis. Plant Cell **26:** 2080-2097

Cutler SR, Ehrhardt DW, Griffitts JS, Somerville CR (2000) Random GFP::cDNA fusions enable visualization of subcellular structures in cells of Arabidopsis at a high frequency. Proc Natl Acad Sci U S A **97:** 3718-3723

Drakakaki G, Dandekar A (2013) Protein secretion: how many secretory routes does a plant cell have? Plant Sci **203-204:** 74-78

Ebine K, Inoue T, Ito J, Ito E, Uemura T, Goh T, Abe H, Sato K, Nakano A, Ueda T (2014) Plant vacuolar trafficking occurs through distinctly regulated pathways. Curr Biol **24:** 1375-1382

Ebine K, Okatani Y, Uemura T, Goh T, Shoda K, Niihama M, Morita MT, Spitzer C, Otegui MS, Nakano A, Ueda T (2008) A SNARE complex unique to seed plants is required for protein storage vacuole biogenesis and seed development of Arabidopsis thaliana. Plant Cell **20:** 3006-3021

Fuji K, Shimada T, Takahashi H, Tamura K, Koumoto Y, Utsumi S, Nishizawa K, Maruyama N, Hara-Nishimura I (2007) Arabidopsis vacuolar sorting mutants (green fluorescent seed) can be identified efficiently by secretion of vacuole-targeted green fluorescent protein in their seeds. Plant Cell **19:** 597-609

Gao C, Luo M, Zhao Q, R. Y, Y. C, Zeng Y, Xia J, Jiang L (2014) A Unique Plant ESCRT Component, FREE1, Regulates Multivesicular Body Protein Sorting and Plant Growth. Current Biology

Geldner N, Denervaud-Tendon V, Hyman DL, Mayer U, Stierhof Y-D, Chory J (2009) Rapid, combinatorial analysis of membrane compartments in intact plants with a multicolor marker set. Plant J **59:** 169-178

Grefen C, Donald N, Hashimoto K, Kudla J, Schumacher K, Blatt MR (2010) A ubiquitin-10 promoter-based vector set for fluorescent protein tagging facilitates temporal stability and native protein distribution in transient and stable expression studies. Plant J **64:** 355-365

Haas TJ, Sliwinski MK, Martínez DE, Preuss M, Ebine K, Ueda T, Nielsen E, Odorizzi G, Otegui MS (2007) The Arabidopsis AAA ATPase SKD1 is involved in multivesicular endosome function and interacts with its positive regulator LYST-INTERACTING PROTEIN5. Plant Cell **19:** 1295-1312

Henne WM, Buchkovich NJ, Emr SD (2011) The ESCRT pathway. Dev Cell **21:** 77-91

Hirano T, Matsuzawa T, Takegawa K, Sato MH (2011) Loss-of-function and gain-of-function mutations in FAB1A/B impair endomembrane homeostasis, conferring pleiotropic developmental abnormalities in Arabidopsis. Plant Physiol **155:** 797-807

Hofius D, Schultz-Larsen T, Joensen J, Tsitsigiannis DI, Petersen NH, Mattsson O, Jorgensen LB, Jones JD, Mundy J, Petersen M (2009) Autophagic components contribute to hypersensitive cell death in Arabidopsis. Cell **137:** 773-783

Isono E, Katsiarimpa A, Muller IK, Anzenberger F, Stierhof YD, Geldner N, Chory J, Schwechheimer C (2010) The deubiquitinating enzyme AMSH3 is required for intracellular trafficking and vacuole biogenesis in Arabidopsis thaliana. Plant Cell **22:** 1826-1837

Katsiarimpa A, Anzenberger F, Schlager N, Neubert S, Hauser MT, Schwechheimer C, Isono E (2011) The Arabidopsis deubiquitinating enzyme AMSH3 interacts with ESCRT-III subunits and regulates their localization. Plant Cell **23:** 3026-3040

Katsiarimpa A, Kalinowska K, Anzenberger F, Weis C, Ostertag M, Tsutsumi C, Schwechheimer C, Brunner F, Huckelhoven R, Isono E (2013) The Deubiquitinating Enzyme AMSH1 and the ESCRT-III Subunit VPS2.1 Are Required for Autophagic Degradation in Arabidopsis. Plant Cell **25:** 2236-2252

Katsiarimpa A, Munoz A, Kalinowska K, Uemura T, Rojo E, Isono E (2014) The ESCRT-III-interacting deubiquitinating enzyme AMSH3 is essential for degradation of ubiquitinated membrane proteins in Arabidopsis thaliana. Plant Cell Physiol **55:** 727-736

Kulich I, Pecenkova T, Sekeres J, Smetana O, Fendrych M, Foissner I, Hoftberger M, Zarsky V (2013) Arabidopsis exocyst subcomplex containing subunit EXO70B1 is involved in autophagy-related transport to the vacuole. Traffic **14:** 1155-1165

Kushnirov VV (2000) Rapid and reliable protein extraction from yeast. Yeast **16:** 857-860

Lam BC, Sage TL, Bianchi F, Blumwald E (2001) Role of SH3 domain-containing proteins in clathrin-mediated vesicle trafficking in Arabidopsis. Plant Cell **13:** 2499-2512

Liu Y, Bassham DC (2012) Autophagy: pathways for self-eating in plant cells. Annu Rev Plant Biol **63:** 215-237

Mukhtar MS, Carvunis AR, Dreze M, Epple P, Steinbrenner J, Moore J, Tasan M, Galli M, Hao T, Nishimura MT, Pevzner SJ, Donovan SE, Ghamsari L, Santhanam B, Romero V, Poulin MM, Gebreab F, Gutierrez BJ, Tam S, Monachello D, Boxem M, Harbort CJ, McDonald N, Gai L, Chen H, He Y, Vandenhaute J, Roth FP, Hill DE, Ecker JR, Vidal M, Beynon J, Braun P, Dangl JL (2011) Independently evolved virulence effectors converge onto hubs in a plant immune system network. Science **333:** 596-601

Nakagawa T, Kurose T, Hino T, Tanaka K, Kawamukai M, Niwa Y, Toyooka K, Matsuoka K, Jinbo T, Kimura T (2007) Development of series of gateway binary vectors, pGWBs, for realizing efficient construction of fusion genes for plant transformation. J Biosci Bioeng **104:** 34-41

Nishizawa K, Maruyama N, Satoh R, Fuchikami Y, Higasa T, Utsumi S (2003) A C-terminal sequence of soybean beta-conglycinin alpha' subunit acts as a vacuolar sorting determinant in seed cells. Plant J **34:** 647-659

Phillips AR, Suttangkakul A, Vierstra RD (2008) The ATG12-conjugating enzyme ATG10 Is essential for autophagic vesicle formation in Arabidopsis thaliana. Genetics **178:** 1339-1353

Raymond CK, Howald-Stevenson I, Vater CA, Stevens TH (1992) Morphological classification of the yeast vacuolar protein sorting mutants: evidence for a prevacuolar compartment in class E vps mutants. Mol Biol Cell **3:** 1389-1402

Reyes FC, Buono R, Otegui MS (2011) Plant endosomal trafficking pathways. Curr Opin Plant Biol **14:** 666-673

Rojo E, Gillmor CS, Kovaleva V, Somerville CR, Raikhel NV (2001) VACUOLELESS1 is an essential gene required for vacuole formation and morphogenesis in Arabidopsis. Dev Cell **1:** 303-310

Sanderfoot AA, Raikhel N (2003) The Secretory System of Arabidopsis. American Society of Plant Biologists

Sanmartín M, Ordóñez A, Sohn EJ, Robert S, Sánchez-Serrano JJ, Surpin MA, Raikhel NV, Rojo E (2007) Divergent functions of VTI12 and VTI11 in trafficking to storage and lytic vacuoles in Arabidopsis. Proc Natl Acad Sci U S A **104:** 3645-3650

Scheuring D, Viotti C, Kruger F, Kunzl F, Sturm S, Bubeck J, Hillmer S, Frigerio L, Robinson DG, Pimpl P, Schumacher K (2011) Multivesicular bodies mature from the trans-Golgi network/early endosome in Arabidopsis. Plant Cell **23:** 3463-3481

Schneeberger K, Hagmann J, Ossowski S, Warthmann N, Gesing S, Kohlbacher O, Weigel D (2009) Simultaneous alignment of short reads against multiple genomes. Genome Biol **10:** R98

Schneeberger K, Ossowski S, Lanz C, Juul T, Petersen AH, Nielsen KL, Jorgensen JE, Weigel D, Andersen SU (2009) SHOREmap: simultaneous

mapping and mutation identification by deep sequencing. Nat Methods **6:** 550-551

Serrazina S, Dias FV, Malho R (2014) Characterization of FAB1 phosphatidylinositol kinases in Arabidopsis pollen tube growth and fertilization. New Phytol **203:** 784-793

Shahriari M, Keshavaiah C, Scheuring D, Sabovljevic A, Pimpl P, Hausler RE, Hulskamp M, Schellmann S (2010) The AAA-type ATPase AtSKD1 contributes to vacuolar maintenance of Arabidopsis thaliana. Plant J **64:** 71-85

Shimada T, Koumoto Y, Li L, Yamazaki M, Kondo M, Nishimura M, Hara-Nishimura I (2006) AtVPS29, a putative component of a retromer complex, is required for the efficient sorting of seed storage proteins. Plant Cell Physiol **47:** 1187-1194

Shimada T, Yamada K, Kataoka M, Nakaune S, Koumoto Y, Kuroyanagi M, Tabata S, Kato T, Shinozaki K, Seki M, Kobayashi M, Kondo M, Nishimura M, Hara-Nishimura I (2003) Vacuolar processing enzymes are essential for proper processing of seed storage proteins in Arabidopsis thaliana. J Biol Chem **278:** 32292-32299

Singh MK, Kruger F, Beckmann H, Brumm S, Vermeer JE, Munnik T, Mayer U, Stierhof YD, Grefen C, Schumacher K, Jurgens G (2014) Protein delivery to vacuole requires SAND protein-dependent Rab GTPase conversion for MVB-vacuole fusion. Curr Biol **24:** 1383-1389

Spitzer C, Reyes FC, Buono R, Sliwinski MK, Haas TJ, Otegui MS (2009) The ESCRT-related CHMP1A and B proteins mediate multivesicular body sorting of auxin carriers in Arabidopsis and are required for plant development. Plant Cell **21:** 749-766

Svenning S, Lamark T, Krause K, Johansen T (2011) Plant NBR1 is a selective autophagy substrate and a functional hybrid of the mammalian autophagic adapters NBR1 and p62/SQSTM1. Autophagy **7:** 993-1010

Thompson AR, Doelling JH, Suttangkakul A, Vierstra RD (2005) Autophagic nutrient recycling in Arabidopsis directed by the ATG8 and ATG12 conjugation pathways. Plant Physiol **138:** 2097-2110

Ueda T, Uemura T, Sato MH, Nakano A (2004) Functional differentiation of endosomes in Arabidopsis cells. Plant J **40:** 783-789

Uemura T, Ueda T, Ohniwa RL, Nakano A, Takeyasu K, Sato MH (2004) Systematic analysis of SNARE molecules in Arabidopsis: dissection of the post-Golgi network in plant cells. Cell Struct Funct **29:** 49-65

van Leeuwen W, Okresz L, Bogre L, Munnik T (2004) Learning the lipid language of plant signalling. Trends Plant Sci **9:** 378-384

Vermeer JE, van Leeuwen W, Tobena-Santamaria R, Laxalt AM, Jones DR, Divecha N, Gadella TW, Jr., Munnik T (2006) Visualization of PtdIns3P dynamics in living plant cells. Plant J **47:** 687-700

Viotti C, Kruger F, Krebs M, Neubert C, Fink F, Lupanga U, Scheuring D, Boutte Y, Frescatada-Rosa M, Wolfenstetter S, Sauer N, Hillmer S, Grebe M, Schumacher K (2013) The endoplasmic reticulum is the main membrane source for biogenesis of the lytic vacuole in Arabidopsis. Plant Cell **25:** 3434-3449

Wada Y, Anraku Y (1992) Genes for directing vacuolar morphogenesis in Saccharomyces cerevisiae. II. VAM7, a gene for regulating morphogenic assembly of the vacuoles. J Biol Chem **267:** 18671-18675

Weigel D, Glazebrook J (2001) Arabidopsis: A Laboratory Manual. Cold Spring Harbor Laboratory

Weßling R, Epple P, Altmann S, He Y, Yang L, Henz SR, McDonald N, Wiley K, Bader KC, Gläßer C, Mukhtar MS, Haigis S, Ghamsari L, Stephans AE, Ecker JR, Vidal M, Jones JDG, Mayer KFX, van Themaat EVL, Weigel D, Schulze-Lefert P, Dangl JL, Panstruga R, Braun P (2014) Convergent Targeting of a Common Host Protein-Network by Pathogen Effectors from Three Kingdoms of Life. Cell Host & Microbe **16:** 364–375

Wickner W (2010) Membrane fusion: five lipids, four SNAREs, three chaperones, two nucleotides, and a Rab, all dancing in a ring on yeast vacuoles. Annu Rev Cell Dev Biol **26:** 115-136

Winter V, Hauser MT (2006) Exploring the ESCRTing machinery in eukaryotes. Trends Plant Sci **11:** 115-123

Wywial E, Singh SM (2010) Identification and structural characterization of FYVE domain-containing proteins of Arabidopsis thaliana. BMC Plant Biol **10:** 157

Yamazaki M, Shimada T, Takahashi H, Tamura K, Kondo M, Nishimura M, Hara-Nishimura I (2008) Arabidopsis VPS35, a retromer component, is required for vacuolar protein sorting and involved in plant growth and leaf senescence. Plant Cell Physiol **49:** 142-156

Yoshimoto K, Hanaoka H, Sato S, Kato T, Tabata S, Noda T, Ohsumi Y (2004) Processing of ATG8s, ubiquitin-like proteins, and their deconjugation by ATG4s are essential for plant autophagy. Plant Cell **16:** 2967-2983

Zhang C, Hicks GR, Raikhel NV (2014) Plant vacuole morphology and vacuolar trafficking. Front Plant Sci **5:** 476

Zhuang X, Wang H, Lam SK, Gao C, Wang X, Cai Y, Jiang L (2013) A BAR-Domain Protein SH3P2, Which Binds to Phosphatidylinositol 3-Phosphate and ATG8, Regulates Autophagosome Formation in Arabidopsis. Plant Cell **25:** 4596-4615

Zouhar J, Rojo E, Bassham DC (2009) AtVPS45 is a positive regulator of the SYP41/SYP61/VTI12 SNARE complex involved in trafficking of vacuolar cargo. Plant Physiol **149:** 1668-1678

Figure legends

Figure 1. The *vfd1(fyve1-2)* mutation causes seedling lethality and defects in central vacuole formation.

(A) and (B) Phenotypes of *vfd1(fyve1-2).* (A) 7-day-old seedlings of *vfd1(fyve1-2)* are shown in comparison to wild-type seedlings at the same age. Scale bars: 0.5 mm. (B) Confocal microscopy images of the vacuolar membrane marker GFP-∂TIP in wild-type (7-day-old) and *vfd1(fyve1-2)* (7-day-old) mutant epidermis cells. (C) Schematic presentation of the FYVE1 domain structure. Position of the *vfd1* mutation (C415T) leading to a premature stop codon (Q139*) is shown.

Figure 2. The transposon insertion line *fyve1-1* shows a similar phenotype as *vfd1.*

(A) Schematic presentation of the transposon insertion site in *fyve1-1*. Gray boxes indicate UTRs, solid boxes indicate exons and lines indicate introns. Forward and reverse primer positions used in (C) are indicated. (B) A 7-day-old seedling of *fyve1-1* is shown in comparison with a wild-type seedling at the same age. Scale bars: 0.5 mm (C) qRT-PCR analysis of *fyve1-1*. Expression of *FYVE1* in wild-type and *fyve1-1* seedlings was analyzed with *FYVE1*- and *ACTIN8*-specific primers. (D) Root morphology of *fyve1-1*. SEM micrographs of wild-type and *fyve1-1* root tips. Scale bars: 100 µm. (E) Confocal microscopy images of the vacuolar membrane marker GFP-∂TIP in 5-day-old wild-type and *vfd1(fyve1-2)* epidermis cells. Scale bars: 10 µm.

Figure 3. Vacuoles in *fyve1-1* show tubular-like interconnected structures.

(A) and (C) Vacuole morphology in 2-day-old wild-type (A) and 5-day-old *fyve1-1* (C) root epidermis cells visualized by BCECF-staining. White boxes indicate the cells used for surface rendering. Scale bars: 10 µm. (B) and (D) Representative 3D surface renderings of wild-type (B) and *fyve1-1* (D) vacuoles in root epidermis cells. Views from the front (left) and the side (right) are shown. Scale bars: 5 µm.

Figure 4. *fyve1* mutants accumulate ubiquitinated proteins in the membrane fraction.

(A) and (B) immunoblots with an anti-ubiquitin P4D1 antibody from total protein extracts. (A) Total extracts of 7-day-old wild type and *vfd1(fyve1-2)* together with two complemented lines of *vfd1(fyve1-2)* were subjected to immunoblotting with anti-ubiquitin antibody. CDC2 was used as a loading control. (B) 7-day-old *fyve1-1* mutants in comparison to wild-type seedlings of the same age were analyzed with an anti-ubiquitin immunoblot. CDC2 was used as a loading control. (C) Total extracts (S13) of 7-day-old *fyve1-1* mutants were fractionated by ultracentrifugation to separate the microsomal- (P100) and soluble fraction (S100) and subjected to immunoblotting using an anti-ubiquitin antibody. Note that the majority of ubiquitinated proteins accumulate in the membrane (P100) fraction. Anti-UGPase and anti-H^+-ATPase antibodies were used for controls for the soluble and membrane fractions, respectively.

Figure 5. *fyve1-1* mutants are impaired in 12S globulin and 2S albumin processing.

(A) Seeds of wild-type (left) together with GFP-CT24-expressing *fyve1-1* homozygous- (middle) or *fyve1-1* heterozygous- and wild-type seeds (right). Scale bar: 1 mm. Seeds were photographed with a binocular microscope (top panel) or a epifluorescent microscope (lower panel). Genotyping results are shown in Supplemental Figure 4. (B) GFP-CT24 in mature embryos of wild type and *fyve1-1*. Note that whereas in wild type, GFP-CT24 signals (green) overlap with the autofluorescence of the seed storage vacuoles (magenta), in *fyve1-1*, GFP-CT24 is secreted into the intercellular spaces. (C) A coomassie–stained gradient gel of total protein extracts of wild type and *fyve1-1* carrying GFP-CT24. p12S: 12S globulin precursors. (D), (E) and (F) Immunoblots of the same extracts using anti-12S globulin, anti-2S albumin and anti-GFP antibodies to detect 12S globulin subunits and 12S globulin precursors (p12S) (C), 2S albumin and 2S albumin precursors (p2S) (E) and GFP-CT24 (F). Asterisk indicates an unspecific band.

Figure 6. *fyve1-1* accumulates autophagosome markers.

Total extracts from wild-type, *fyve1-1*, *atg7-2* and *atg10-1* seedlings grown under long-day conditions were subjected to immunoblotting using an anti-NBR1 and an anti-ATG8 antibody. CDC2 was used as a loading control.

Figure 7. GFP-FYVE1 colocalizes with ARA7.

(A) Localization of GFP-FYVE1 and mRFP-SYP43 in 5-day-old root epidermis cells. The percentage of GFP-SH3P2 vesicle colocalizing with mRFP-SYP43 is indicated at the bottom of the panel. Total number of GFP-FYVE1 vesicle counted were n=257. (B) and (C) Localization of GFP-FYVE1 and mRFP-SYP43 upon 45 minutes of BFA treatment. Magnification of a BFA-body in the area indicated in (B) is shown in (C). Note that mRFP-SYP43, but not GFP-FYVE1, localizes to BFA-bodies. (D) Localization of GFP-FYVE1 and mCherry-ARA7 in 5-day-old root epidermis cells. The percentage of GFP-SH3P2 vesicle colocalizing with mCherry-ARA7 is indicated at the bottom of the panel. Total number of GFP-FYVE1 vesicle counted were n=253. (E) and (F) Localization of GFP-FYVE1 and mCherry-ARA7and upon 45 minutes of Wortmannin (WM) treatment. Magnification of a WM-compartment in the area indicated in (E) is shown in (F). Note that both proteins localize to WM-compartments. (G) Total extracts (S13) from wild type and complementing GFP-FYVE1 line were subjected to ultracentrifugation to separate soluble (S100) and microsomal (P100)

fractions. Proteins from each fraction were subjected to immunoblotting using anti-FYVE1. Anti-UGPase and anti-H^+-ATPase antibodies were used for controls for soluble and membrane fractions, respectively.

Figure 8. FYVE1 interacts with SH3P2 and SH3P3.

Y2H analysis of GAD-FYVE1(ΔFYVE) with GBD-fused SH3P2 and SH3P3. Transformants were grown on SC-LW or SC-LWH plates with the indicated amount of 3-AT to test their auxotrophic growth. The expression of all fusion proteins was verified by immunoblotting (Supplemental Figure 3).

Figure 9. FYVE1 colocallizes with SH3P2 on SKD1(EQ)-induced class E compartments.

(A) to (C) GFP-SH3P2 expressing plants were crossed with CLC-mKO (A), mRFP-SYP43 (B) and mCherry-ARA7 (C) expressing lines. Colocalization was analyzed in root epidermis cells of 5-day-old seedlings. The percentage of GFP-SH3P2 vesicle colocalizing with each marker is presented at the bottom of each panel. Total number of GFP-SH3P2 vesicle counted were n=619 for (A), n=162 for (B) and n=158 for (C). (D) and (F) Co-expression analysis of SH3P2-GFP with mCherry-ARA7 in Arabidopsis cell culture-derived protoplasts. Cells in (E) were treated with Wortmannin (WM) for 120 minutes before observation. Note that whereas mCherry-ARA7 accumulates in WM-induced compartments, GFP-SH3P2 does not. Magnification of a WM-compartment in the area indicated in (E) is shown in (F). (G) to (I) Co-expression of SH3P2-GFP and mCherry-AMSH3 with SKD1(WT) (G) or SKD1(EQ) (H) in Arabidopsis cell culture–derived protoplasts. Note that a fraction of GFP-SH3P2 colocalizes with mCherry-AMSH3 in SKD1(EQ)-induced class E compartments. Magnification of a class E compartment in the area indicated in (H) is shown in (I). (J) and (K) Localization of GFP-SH3P2 with TagRFP-FYVE1 upon co-expression of SKD1(EQ) in an Arabidopsis root-derived protoplast. Magnification of a class E compartment in the area indicated in (J) is shown in (K).

Figure 10. FYVE1 localizes to late endosomes and regulate intracellular trafficking and vacuole biogenesis.

FYVE1 localizes to late endosomes and interacts with SH3P2. FYVE1 function together with SH3P2 or with other interactors is essential for endocytic protein

degradation, vacuolar protein transport, autophagy and vacuole biogenesis. Lack of FYVE1 causes seedling lethality, indicating that FYVE1 is essential for plant growth and development.

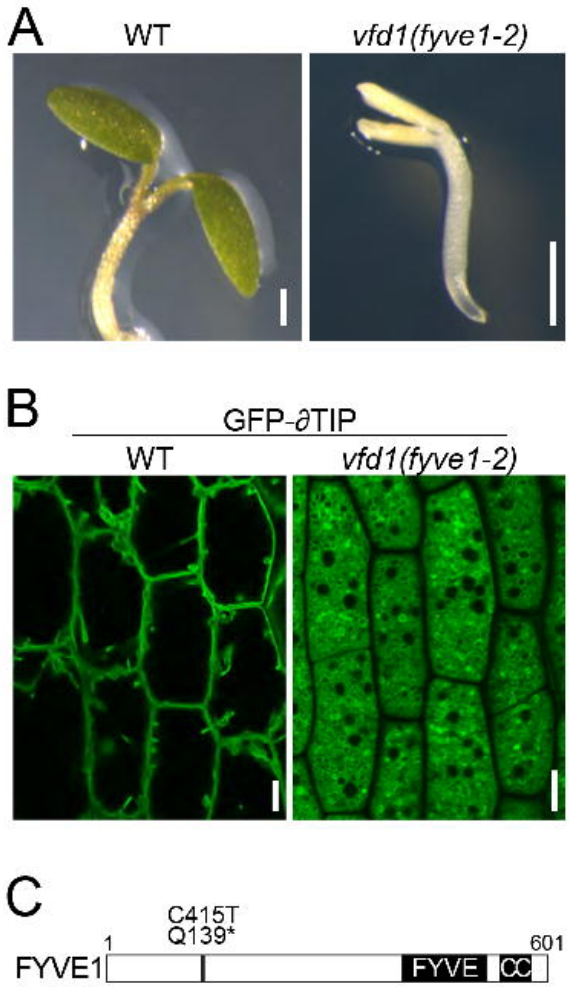

Figure 1. The *vfd1(fyve1-2)* mutation causes seedling lethality and defects in central vacuole formation.

(A) and (B) Phenotypes of *vfd1(fyve1-2)*. (A) 7-day-old seedlings of *vfd1(fyve1-2)* are shown in comparison to wild-type seedlings at the same age. Scale bars: 0.5 mm. (B) Confocal microscopy images of the vacuolar membrane marker GFP-∂-TIP in 5-day-old wild-type and *vfd1(fyve1-2)* epidermis cells. Scale bars: 10 µm. (C) Schematic presentation of the FYVE1 domain structure. Position of the *vfd1* mutation (C415T) leading to a premature stop codon (Q139*) is shown.

Figure 1

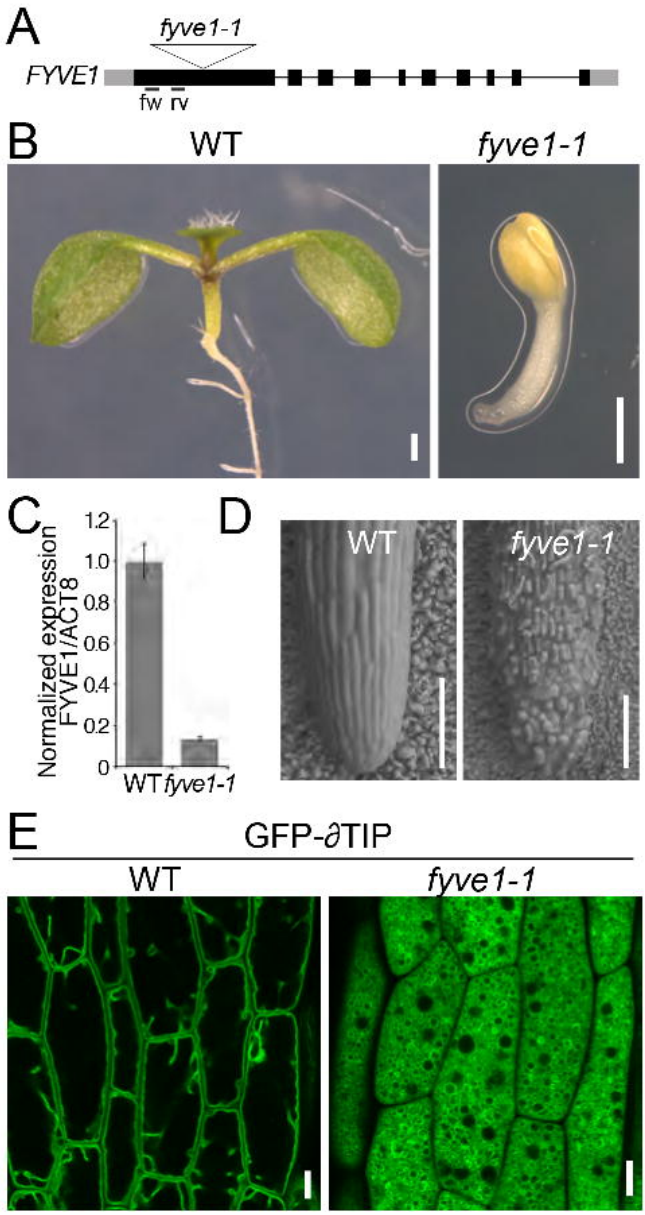

Figure 2. The T-DNA insertion line *fyve1-1* shows a similar phenotype like *vfd1*.

(A) Schematic presentation of the T-DNA insertion site in *fyve1-1*. Gray boxes indicate UTRs, solid boxes indicate exons and lines indicate introns. Forward and reverse prier positions used in (C) is indicated. (B) A 7-day-old seedling of *fyve1-1* is shown in comparison with a wild-type seedling at the same age. Scale bars: 0.5 mm (C) qRT-PCR analysis of *fyve1-1*. Expression of *FYVE1* in wild-type and *fyve1-1* seedlings was analyzed with *FYVE1*- and *ACTIN8*-specific primers. (D) Root morphology of *fyve1-1*. SEM micrographs of wild-type and *fyve1-1* root tips. Scale bars: 100 µm. (E) Confocal microscopy images of the vacuolar membrane marker GFP-∂TIP in 5-day-old wild-type and *vfd1(fyve1-2)* epidermis cells. Scale bars: 10 µm.

Figure 2

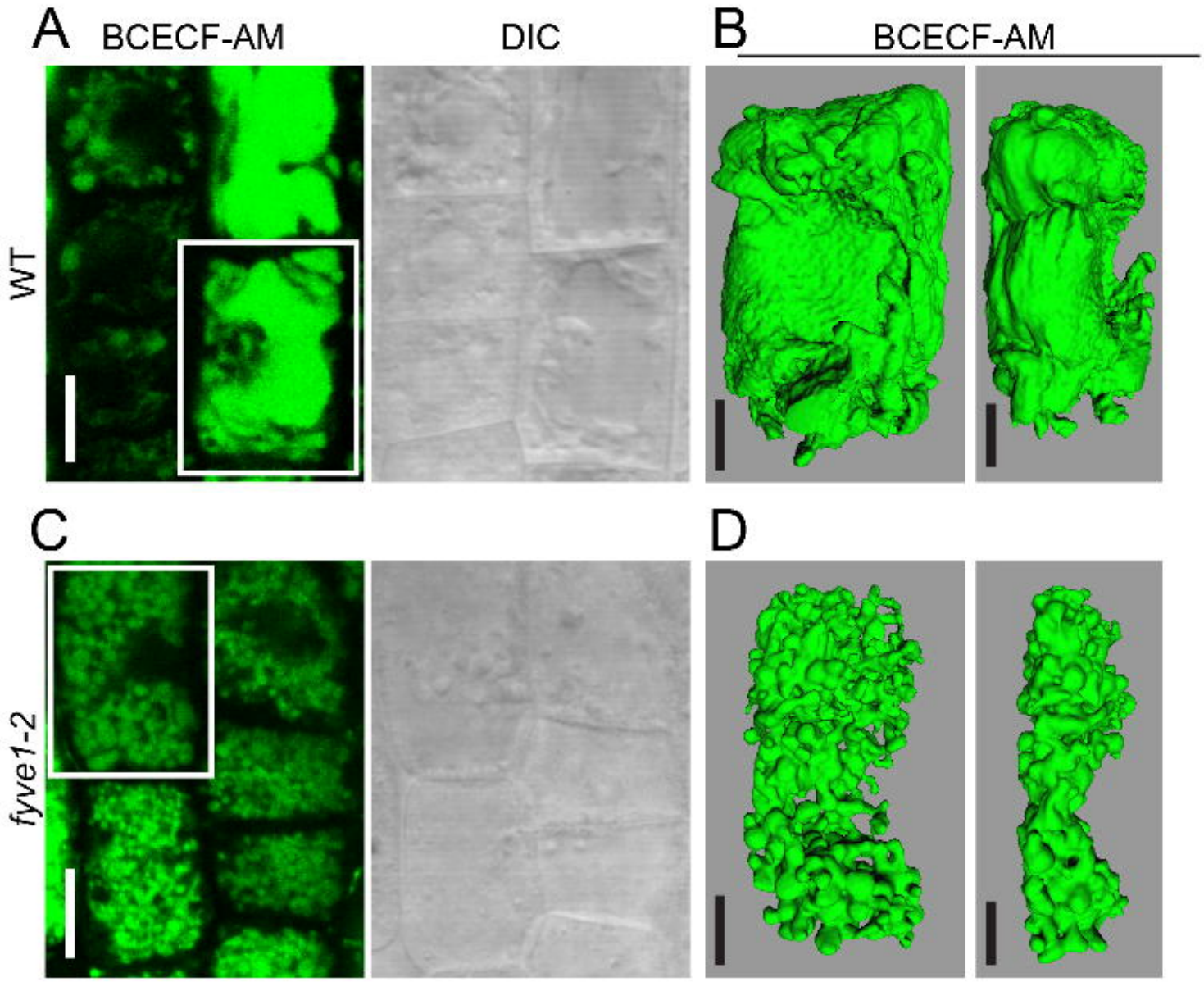

Figure 3. Vacuoles in *fyve1-1* show tubular-like interconnected structures.

(A) and (C) Vacuole morphology in 2-day-old wild-type (A) and 5-day-old *fyve1-1* (C) root epidermis cells visualized by BCECF-staining. White boxes indicate the cells used for surface rendering. Scale bars: 10 μm. (B) and (D) Representative 3D surface renderings of wild-type (B) and *fyve1-1* (D) vacuoles in root epidermis cells. Views from the front (left) and the side (right) are shown. Scale bars: 5 μm.

Figure 3

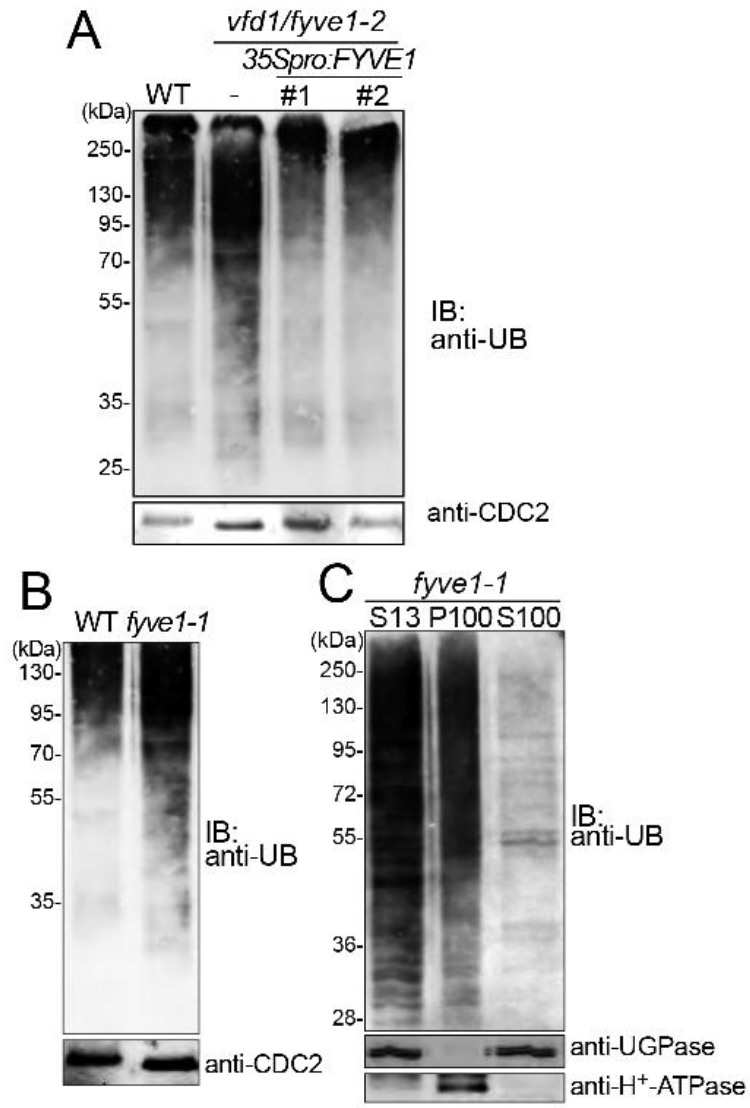

Figure 4. *fyve1* mutants accumulate ubiquitinated proteins in the membrane fraction.

(A) and (B) immunoblots with an anti-ubiquitin P4D1 antibody from total protein extracts. (A) Total extracts of 7-day-old wild type and *vfd1(fyve1-2)* together with two complemented lines of *vfd1(fyve1-2)* were subjected to immunoblotting with anti-ubiquitin antibody. CDC2 was used as a loading control. (B) 7-day-old *fyve1-1* mutants in comparison to wild-type seedlings of the same age were analyzed with an anti-ubiquiti immunoblot. CDC2 was used as a loading control. (C) Total extracts (S13) of 7-day-old *fyve1-1* mutants were fractionated by ultracentrifugation to separate the microsomal fraction (P100) and soluble fraction (S100) and subjected to immunoblotting using an anti-ubiquitin antibody. Note that the majority of ubiquitinated proteins accumulate in the membrane (P100) fraction. Anti-UGPase and anti-H^+-ATPase antibodies were used for controls for the soluble and membrane fractions, respectively.

Figure 4

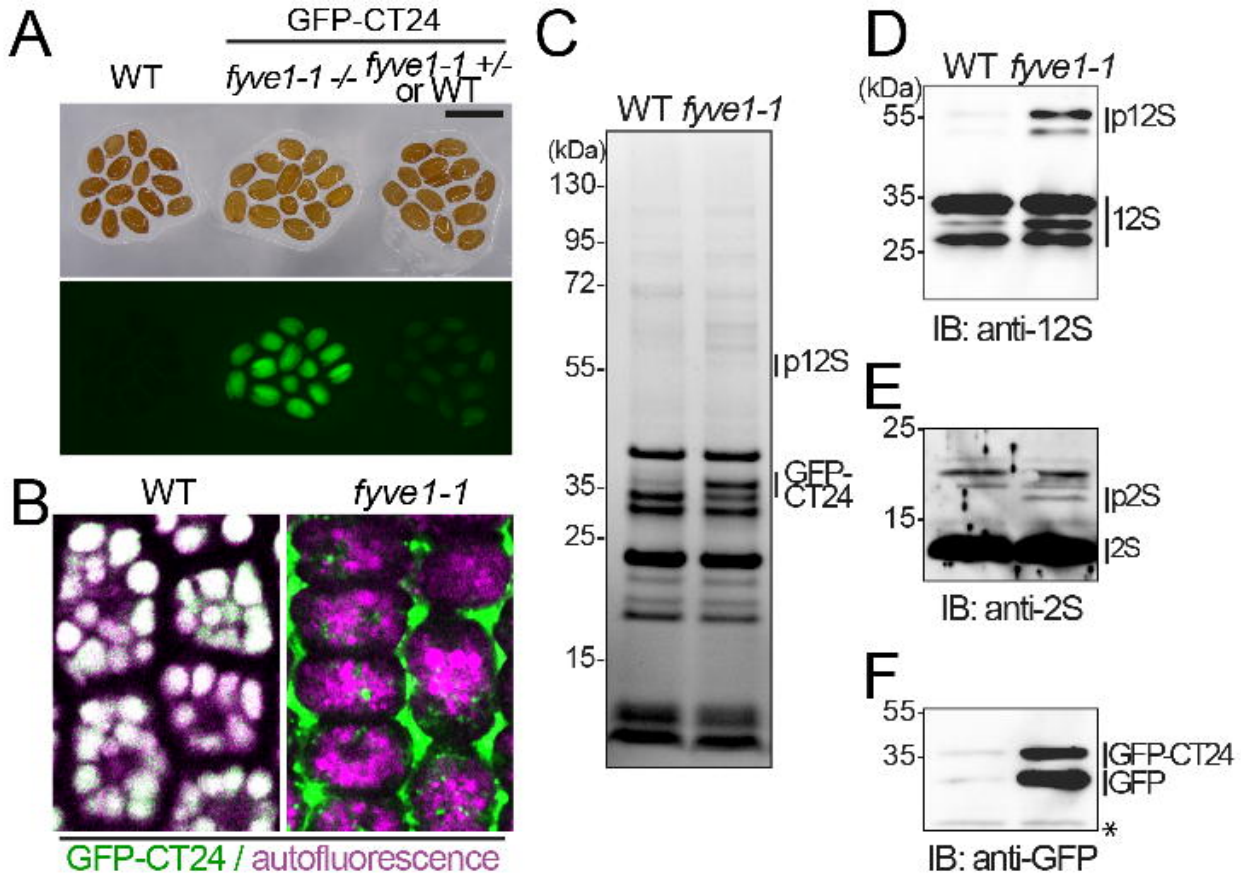

Figure 5. *fyve1-1* mutants are impaired in 12S globulin and 2S albumin processing.

(A) Seeds of wild-type (left) together with GFP-CT24-expressing *fyve1-1* homozygous- (middle) or *fyve1-1* heterozygous- and wild-type seeds (right). Scale bar: 1 mm. Seeds were photographed with a binocular microscope (top panel) or a epifluorescent microscope (lower panel). Genotyping results are shown in Supplemental Figure 4. (B) GFP-CT24 in mature embryos of wild type and *fyve1-1*. Note that whereas in wild type, GFP-CT24 signals (green) overlap with the autofluorescence of the seed storage vacuoles (magenta), in *fyve1-1*, GFP-CT24 is secreted into the intercellular spaces. (C) A coomassie -stained gradient gel of total protein extracts of wild type and *fyve1-1* carrying GFP-CT24. p12S: 12S globulin precursors. (D), (E) and (F) Immunoblots of the same extracts using anti-12S globulin, anti-2S albumin and anti-GFP antibodies to detect 12S globulin subunits and 12S globulin precursors (p12S) (C), 2S albumin and 2S albumin precursors (p2S) (E) and GFP-CT24 (F). Asterisk indicates an unspecific band.

Figure 5

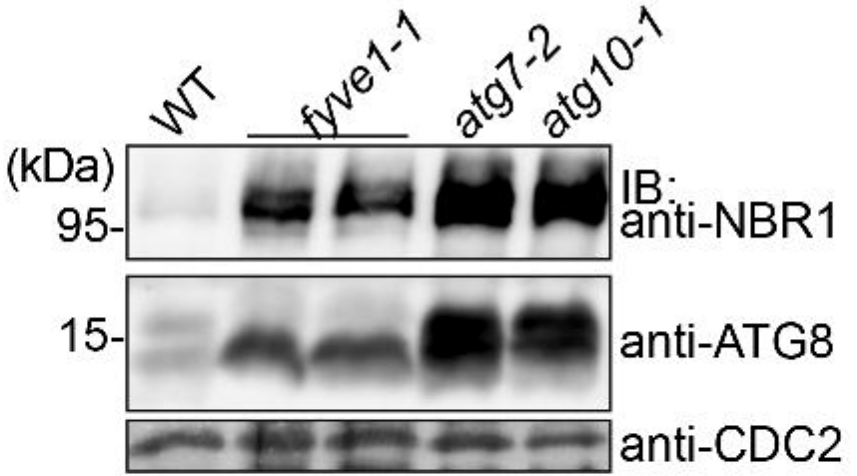

Figure 6. *fyve1-1* accumulates autophagosome components ATG8 and NBR1.

Total extracts from 7-day-old wild-type, *fyve1-1, atg7-2 and atg10-1* seedlings grown under long-day conditions were subjected to immunoblotting using an anti-NBR1 and an anti-ATG8 antibody. CDC2 was used as a loading control.

Figure 6

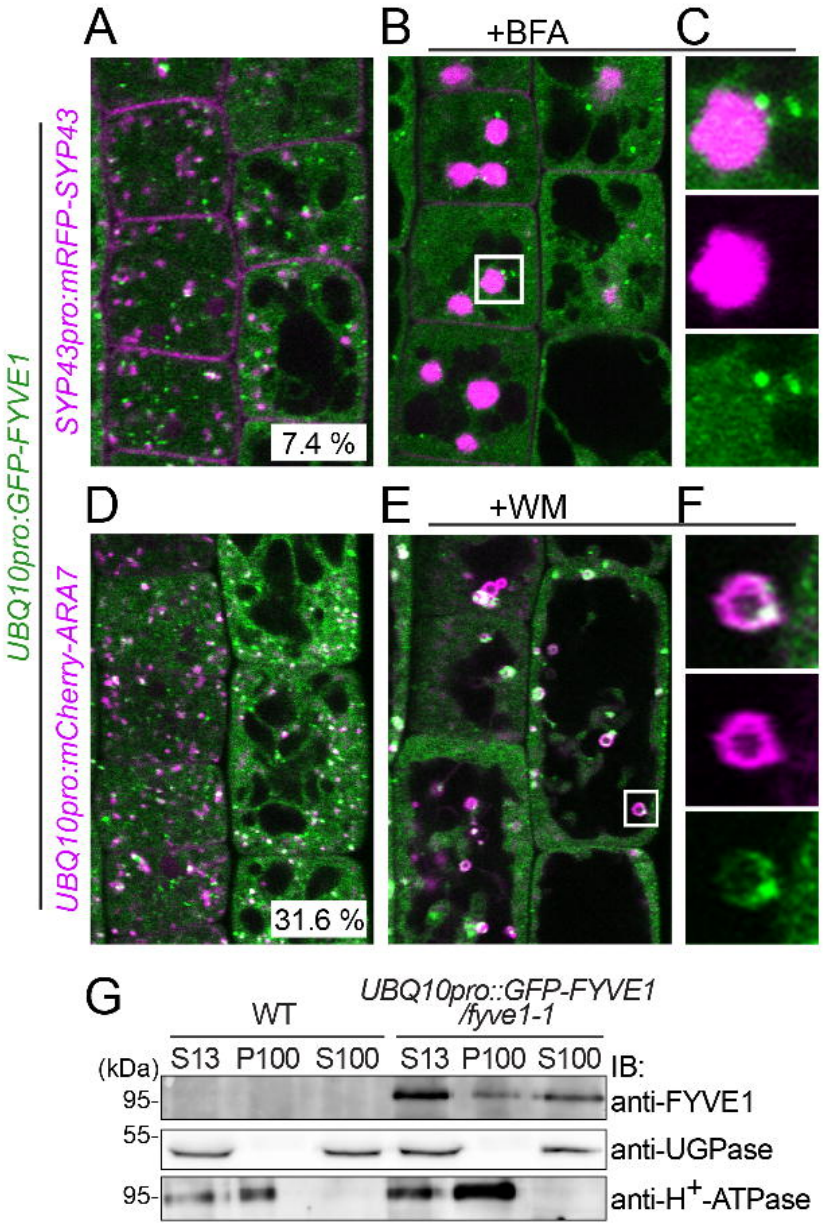

Figure 7. GFP-FYVE1 colocalizes with the late endosome marker ARA7. (A) Localization of GFP-FYVE1 and mRFP-SYP43 in 5-day-old root epidermis cells. The percentage of GFP-SH3P2 vesicle colocalizing with mRFP-SYP43 is indicated at the bottom of the panel. Total number of GFP-FYVE1 vesicle counted were n=257. (B) and (C) Localization of GFP-FYVE1 and mRFP-SYP43 upon 45 minutes of BFA treatment. Magnification of a BFA-body in the area indicated in (B) is shown in (C). Note that mRFP-SYP43 , but not GFP-FYVE1, localizes to BFA-bodies. (D) Localization of GFP-FYVE1 and mCherry-ARA7 in 5-day-old root epidermis cells. The percentage of GFP-SH3P2 vesicle colocalizing with mCherry-ARA7 is indicated at the bottom of the panel. Total number of GFP-FYVE1 vesicle counted were n=253. (E) and (F) Localization of GFP-FYVE1 and mCherry-ARA7and upon 45 minutes of Wortmannin (WM) treatment. Magnification of a WM-compartment in the area indicated in (E) is shown in (F). Note that both proteins localize to WM-compartments. (G) Total extracts (S13) from wild type and *fyve1-1* line complemented by GFP-FYVE1 line were subjected to ultracentrifugation to separate soluble (S100) and microsomal (P100) fractions. Proteins from each fraction were subjected to immunoblotting using anti-FYVE1. Anti-UGPase and anti-H^+-ATPase antibodies were used for controls for soluble and membrane fractions, respectively.

Figure 7

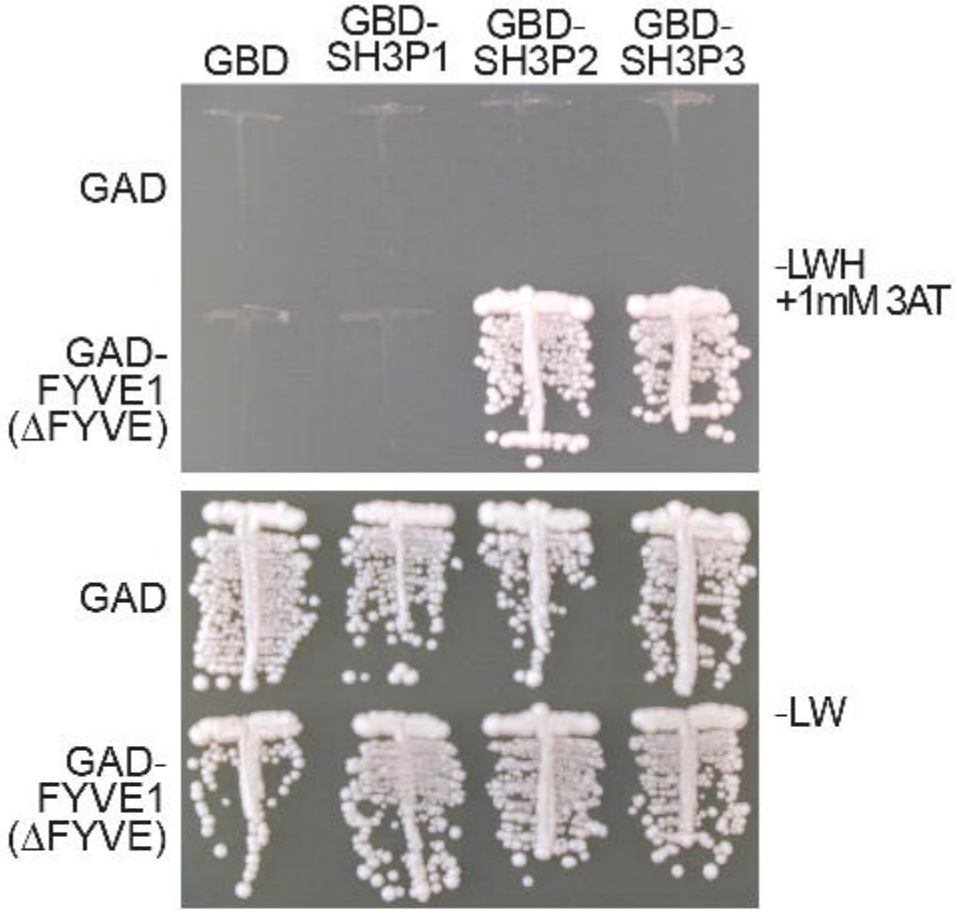

Figure 8. FYVE1 interacts with SH3P2 and SH3P3.
Y2H analysis of GAD-FYVE1(ΔFYVE) with GBD-fused SH3P1, SH3P2 and SH3P3. Transformants were grown on a SC-LW or SC-LWH plate supplemented with 1 mM 3-AT to test their auxotrophic growth. The expression of all fusion proteins was verified by immunoblotting (Supplemental Figure 3).

Figure 8

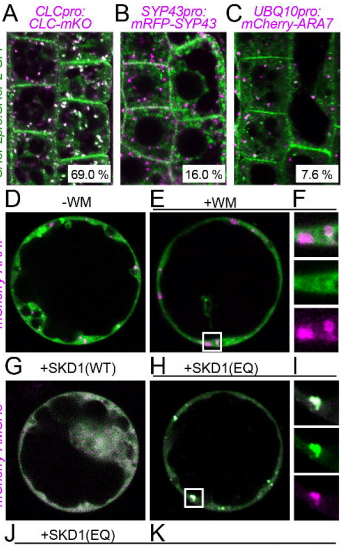

Figure 9. FYVE1 colocallizes with SH3P2 on SKD1(EQ)-induced class E compartments.
(A) to (C) GFP-SH3P2 expressing plants were crossed with CLC-mKO (A), mRFP-SYP43 (B) and mCherry-ARA7 (C) expressing lines. Colocalization was analyzed in root epidermis cells of 5-day-old seedlings. The percentage of GFP-SH3P2 vesicle colocalizing with each marker is presented at the bottom of each panel. Total number of GFP-SH3P2 vesicle counted were n=619 for (A) n=162 for (B) and n=158 for (C). (D) to (F) Coexpression analysis of SH3P2-GFP with mCherry-ARA7 in Arabidopsis cell culture-derived protoplasts. Cells in (E) were treated with Wortmannin (WM) for 120 minutes before observation. Note that whereas mCherry-ARA7 accumulates in WM-induced compartments, GFP-SH3P2 does not. Magnification of a WM-compartment in the area indicated in (E) is shown in (F). (G) to (I) Coexpression of SH3P2-GFP and mCherry-AMSH3 with SKD1(WT) (G) or SKD1(EQ) (H) in Arabidopsis cell culture–derived protoplasts. Note that a fraction of GFP-SH3P2 colocalizes with mCherry-AMSH3 in SKD1(EQ)-induced class E compartments. Magnification of a class E compartment in the area indicated in (H) is shown in (I). (J) and (K) Localizations of GFP-SH3P2 with TagRFP-FYVE1 upon coexpression of SKD1(EQ) in an Arabidopsis root-derived protoplast. Magnification of a class E compartment in the area indicated in (J) is shown in (K).

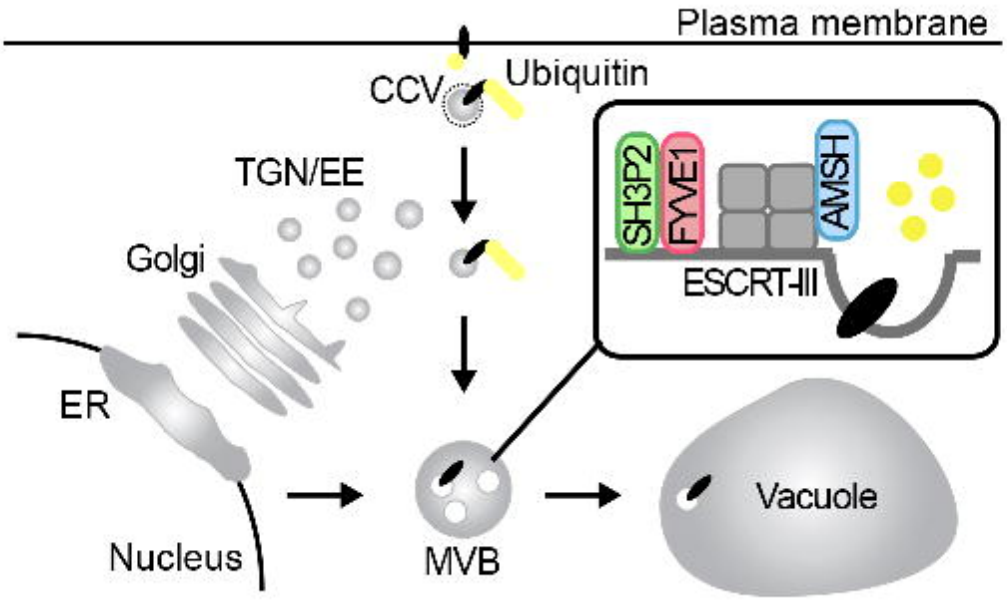

Figure 10. FYVE1 localizes to late endosomes and regulate intracellular trafficking and vacuole biogenesis.

FYVE1 localizes to late endosomes and interacts with SH3P2. FYVE1 function together with SH3P2 or with other interactors is essential for endocytic protein degradation, vacuolar protein transport, autophagy and vacuole biogenesis. Lack of FYVE1 causes seedling lethality, indicating that FYVE1 is essential for plant growth and development

Figure 10

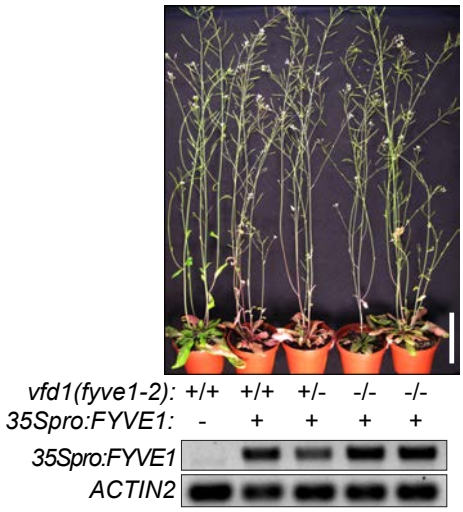

Supplemental Figure 1. Complementation of the *vfd1(fyve1-2)* mutant. Photographs of *vfd1/fyve1-2* mutant lines that express a *35Spro:FYVE1* construct are shown in comparison to wild-type plant at the same age (upper panel). Expression of the transgene was verified by RT-PCR using transgene- and *ACTIN2*-specific primers (bottom panel). Scale bar: 6 cm.

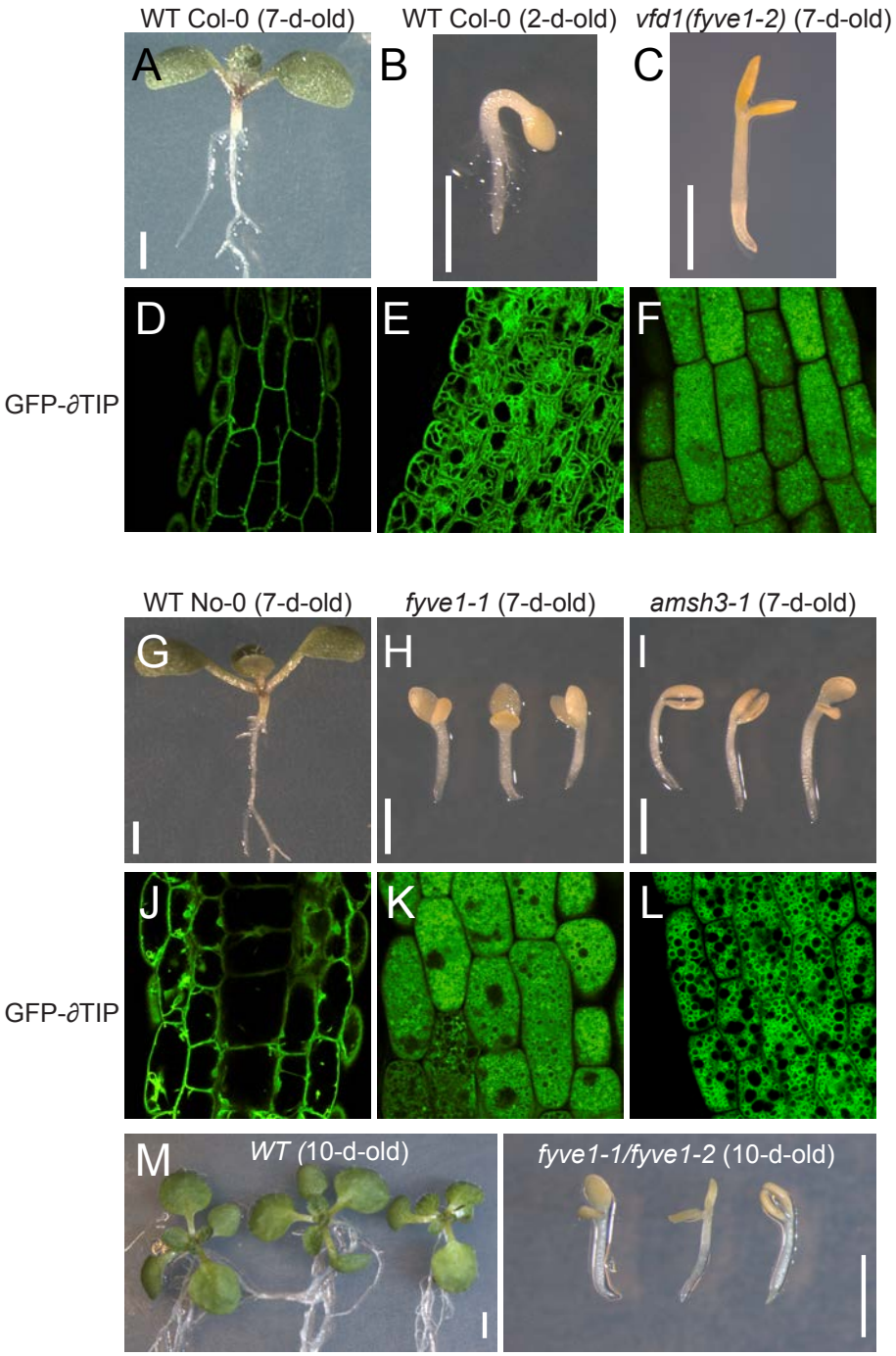

Supplemental Figure 2. Seedling- and vacuole phenotypes of *fyve1-1*, *fyve1-2* and *amsh3-1*.

(A to F) Photographs of the seedling and vacuole phenotypes of 7-day-old (A and D) and 2-day-old (B and E) wild type (Col-0) and 7-day-old *vfd1fyve1-2* mutant (C and F) are shown. Note that the *vfd1/fyve1-2* seedling is approximately the size of a 2-day-old wild-type seedling. Vacuolar membranes of the seedlings are visualized with the GFP=∂TIP mareker. (G to L) Photographs of the seedling and vacuole phenotypes of 7-day-old wild type (No-0) (G and J), 7-day-old *fyve1-1* (H and K) and 7-day-old *amsh3-1* (I and L) are shown. Scale bars: 1mm. (M) Transheterozygous *fyve1-1/fyve1-2* mutants show the same seedling lethal phenotype as the *fyve1-1-, fyve1-2* homozygous mutants. Scale bars: 2 mm.

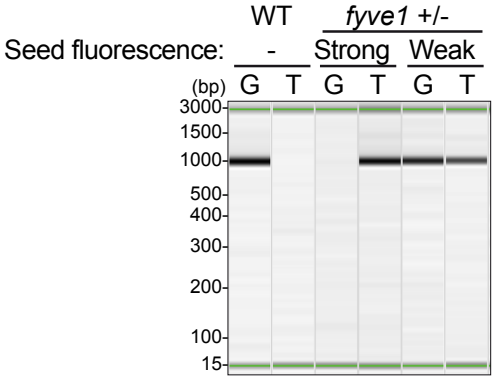

Supplemental Figure 3. Seeds with strong green fluorescence are homozygous for the *fyve1-1* transposon insertion.

PCR-based genotyping analysis was conducted using genomic DNA extracted from seeds from wild type or a *fyve1-1* heterozygous plant containing GFP-CT24. Among the seeds derived from a heterozygous mother plant, seeds with strong and weak green fluorescence observed. 10 seeds from each population shown in Figure 5A were subjected to genotyping analysis. Lanes G indicate gene-specific PCR products and Lanes T indicate transposon-specific PCR products. Note that the pool of strongly fluorescing seeds acorrespond to homozygous *fyve1-1*.

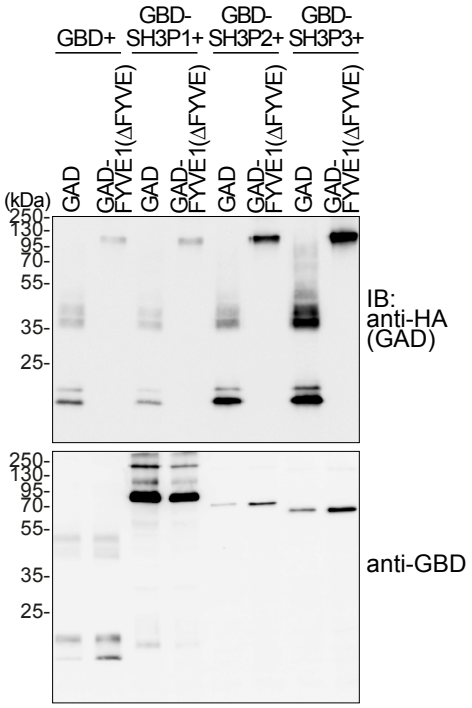

Supplemental Figure 4. Expression of the constructs used for YTH analysis.

Immunoblot of yeast total protein extracts from yeast cells used in Figure 8. Anti-HA and anti-GBD antibodies were used to detect GAD- and GBD-fused proteins, respectively. The GAD-fusion vector pGADT7 contains an HA-tag enabling the detection of the fusion protien with an anti-HA antibody.

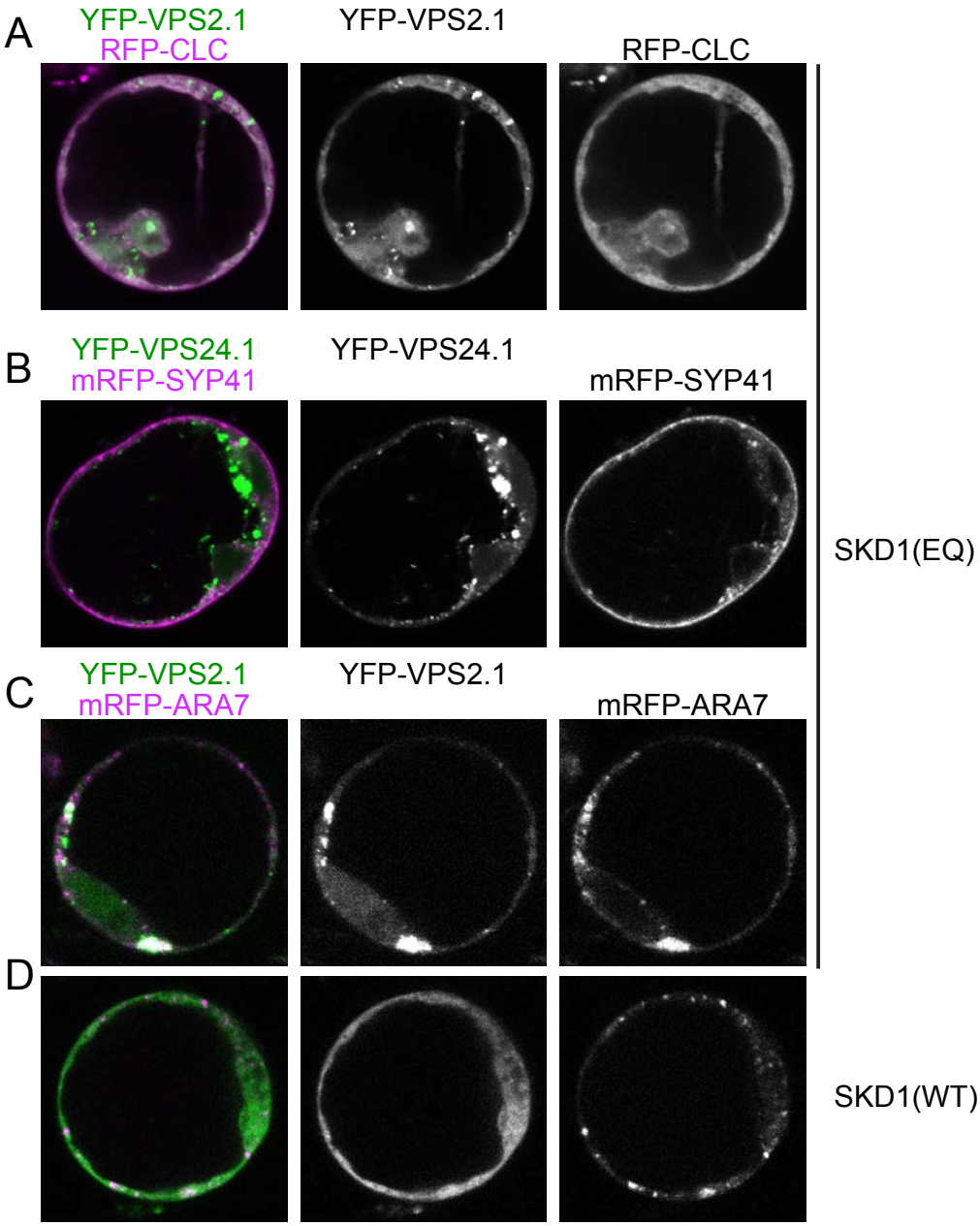

Supplemental Figure 5. Coexpression of SKD1(EQ) specifically affect the late endosomal marker ARA7.
Localization of ESCRT-III subunits YFP-VPS2.1 or YFP-VPS24.1 together with RFP-CLC (A), the TGN/early endosome-marker mRFP-SYP43 (B) and the late endosome marker mRFP-ARA7 (C) upon co-expression with SKD1 (EQ). Localization of YFP-VPS2.1 and mRFP-ARA7 upon coexpression with SKD1(WT) is shown in (D). Note that only mRFP-ARA7 relocates to the SKD1(EQ)-induced class-E compartments together with the ESCRT-III subunit VPS2.1.

Supplemental Table 1: Primers used in this study

Primer	Sequence
CK40 FYVE1 GW fw	GGGGACAAGTTTGTACAAAAAAGCAGGCTATGCAACA GGGAGATTAC
CK41 FYVE1 GW fw	GGGGACCACTTTGTACAAGAAAGCTGGGTTCAATGTG CGCTAACGAG
CK131 FYVE1 GW fw	GGGGACAAGTTTGTACAAAAAAGCAGGCTTGCAACAG GGAGATTAC
CK140 ΔFYVE fw	GGCATTACTCAACCTATTAACAGGCTTTAT
CK141ΔFYVE rv	ATAAAGCCTGTTAATAGGTTGAGTAATGCC
EI511 Genotyping fw	GCGACATCACTAAACCC
EI512 Genotyping rv	AACCCACCAACATAAGAAC
EI528 FYVE fw Bam	AAGGGGATCCGCAACCGTAGCTGGTC
EI529 FYVE rv Sal	AAGGGTCGACAAAGCTAATGGATCGTCC
EI541 tFYVE1 qRT fw	GCAACAGGGAGATTACAATTCG
EI542 tFYVE1 qRT rv	TCGGAGTAGGATTTTGAAATTGA
MN53 SH3P2 GW fw	AAAAAGCAGGCTATGGATGCAATTAGAAAACA
MN54 SH3P2 GW rv	AGAAAGCTGGGTTGAAAACTTCGGACACTTTG
MN215 SH3P1 fw NcoI	AAGGCCATGGTGATCATCACAATCATC
MS8 SH3P1 rv XhoI	GGAACTCGAGTCACTGTTGCTTGGAGTT
MS9 SH3P3 fw EcoRI	GGAAGAATTCATGGATGCGTTTAGAAGAC
MS10 SH3P3 rv SalI	GGAAGTCGACTCAGTAAACTTCAGCAGCA
MS11 SH3P2 fw EcoRI	GGAAGAATTCAGTGATGCAATTAGAAAACA
MS12 SH3P2 rv SalI	GGAAGTCGACTCAGAAAACTTCGGACACT
SH3P2-up5 fw	CACCCACACCAATGGCGACATAAC
SH3P2-dw3 rv	CTATCAAATAAAAGAAGATCC
VC11 FYVE1(ΔFYVE) fw BamHI	AAGGGGATCCGTATGCAACAGGGAGATTACA
VC12 FYVE1(ΔFYVE) rv SalI	AAGGGTCGACTCAATGTGCGCTAACG
ACTIN fw	GGGCTGTTTTTCCCA
ACTIN rv	GGCCTTGGAGATCCA
Ds5-2a	TCCGTTCCGTTTTCGTTTTTTAC